A decentralized framework for self-healing in hydrogen-integrated energy systems

Chen, Jie; Gu, Weiyu; Alharthi, Yahya Z.; Huang, Shoujun; Mansouri, Seyed Amir

DOI
10.1016/j.energy.2025.137033

Publication date
2025

Document Version
Final published version

Published in
Energy

Energy 331 (2025) 137033

Contents lists available at ScienceDirect

Energy

journal homepage: www.elsevier.com/locate/energy

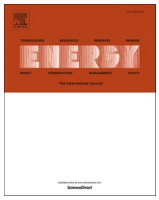

A decentralized framework for self-healing in hydrogen-integrated energy systems

Jie Chen [a], Weiyu Gu [b,*], Yahya Z. Alharthi [c], Shoujun Huang [d], Seyed Amir Mansouri [e]

[a] School of Innovation and Entrepreneurship Education, Chongqing University of Posts and Telecommunications, Chongqing, 400065, China
[b] School of Economics, Central University of Finance and Economics, Beijing, 100081, China
[c] Department of Electrical Engineering, College of Engineering, University of Hafr Albatin, Hafr Al Batin, 39524, Saudi Arabia
[d] International School of Business & Finance, Sun Yat-Sen University, Zhuhai, 519082, China
[e] Department of Engineering Systems & Services, Faculty of Technology, Policy & Management, Delft University of Technology, Delft, The Netherlands

ARTICLE INFO

Keywords:
Coupled power and gas networks
Industrial parks
Power-to-hydrogen technologies
Charging stations
Alternating direction method of multipliers

ABSTRACT

The increasing frequency of environmental events driven by global warming poses a significant threat to smart network operations, highlighting the need for advanced self-healing techniques to enhance grid stability and accelerate recovery during emergencies. This study proposes a two-stage distributed optimization mechanism for self-healing in coupled electricity and gas networks. The mechanism leverages the capabilities of smart prosumers, such as industrial parks, charging stations, and power-to-hydrogen (P2H) units, to minimize load shedding and bolster resilience under emergency conditions. In the first stage, the distribution system operator optimally reconfigures electricity and gas networks, plans distribution feeder operations, and deploys fuel cell-equipped trucks to allocate the required power and gas capacities to smart prosumers via signal pulses. The second stage focuses on modeling the smart prosumers, enabling them to offer their available capacities to the network operator in response to these signals. To ensure secure convergence with minimal information exchange between the two stages, an augmented Alternating Direction Method of Multipliers (ADMM) algorithm is utilized. The proposed mechanism was validated on two different test systems, solved using the GUROBI solver within GAMS. Simulation results demonstrate that the mechanism effectively harnesses maximum capacities from smart prosumers, reducing load shedding by 64.08 % and improving the resilience index by 80.34 %. Furthermore, the augmented ADMM enhanced computational efficiency, achieving a 45.3 % faster solution compared to the standard version while ensuring global optimality.

Nomenclature

Abbreviations	
ADMM	Alternating Direction Method of Multipliers
CB	Capacitor Bank
CHP	Combined Heat and Power
CS	Charging Station
DER	Distributed Energy Resource
DFR	Distribution Feeder Reconfiguration
DU	Distributed unit
EH	Electric Heater
ES	Energy Storage
EV	Electric Vehicle
FC	Fuel Cell
GB	Gas Boiler
GS	Gas Storage
HS	Hydrogen Storage
HU	Hydrogen Unit
IoT	Internet-of-Things
IP	Industrial Park
P2H	Power-To-Hydrogen
SU	Solar Unit
TS	Thermal Storage
VPP	Virtual Power Plant
WU	Wind Unit
Sets	
cs	Charging station index
k	Compressor gain index
es	Electrical storage index
i	Electrical/Gas node index
l	Electrical/Pipe/Travel path index

(continued on next column)

(continued)

(continued on next page)

* Corresponding author.
E-mail addresses: guweiyumake@163.com (W. Gu), s.mansouri@tudelft.nl (S.A. Mansouri).

https://doi.org/10.1016/j.energy.2025.137033
Received 11 March 2025; Received in revised form 10 May 2025; Accepted 6 June 2025
Available online 10 June 2025

(*continued*)

gs	Gas storage index
g	Distributed unit index
hs	Hydrogen storage index
ip	Industrial park index
hu	P2H unit index
n	Scaling index
s	Solar unit index
ts	Thermal storage index
t	Time index
w	Wind unit index

Scalar

$A\text{-}F$	Coefficients of CHP gas consumption function
Δt	Time gap (h)
δ	ADMM stopping criteria
η_{ge}^{DU}	DU energy conversion factor (m^3/kW)
η^{SU}	SU efficiency (%)
η^{Ch}/ η^{Dis}	Charging/Discharging efficiency (%)
η^{FC}	FC efficiency (%)
η_{gh}^{GB}	GB energy conversion factor (m^3/kW)
η^{EL}	EL efficiency (%)
IR^{STC}	Standard sun irradiance (kW/m^2)
LHV^{H2}	Low heat value of hydrogen (kW/kg)
M	Big positive number
N^{CHP}	Number of discrete ranges
$\pi^{Product}$	Product price of industrial units ($/item)
$\pi^{H2,Price}$	Hydrogen price ($/kg)
R^{H2}	Hydrogen constant [kW/(mol.K)]
T^{H2}	Internal temperature of the hydrogen tank (K)
V^{H2}	Molar mass of hydrogen (kg/mol)
$\prod^{Depot}$	Depot location
ω^{Normal}/ $\omega^{Critical}$	Penalty weight of normal/critical loads
$\Upsilon^{SU/WU}$	Power factor range of SU/WU converters
γ^{CHP}	Reactive rate factor of CHP (%)
χ^{T1-T6}	Coefficients for reactive power used by industrial processes

Parameters

α_k^C	Scaling factor
B_l/ G_l/ R_l	Susceptance/conductance/resistance of electric lines (p.u)
C_l^2	Constant of pipelines
$\Delta M5_{ip,t}^{Product,\min}$/ $\Delta M5_{ip,t}^{Product,max}$	Production changes in industrial parks (item)
$\Delta H2_{hu,t}^{Customers,min}$/ $\Delta H2_{hu,t}^{Customers,max}$	Hydrogen consumption changes in P2H units (kg)
$\Delta P_{cs,t}^{Charger,\min}$/ $\Delta P_{cs,t}^{Charger,\max}$	power consumption changes in charging stations (kW)
δ_i^{Min}/ δ_i^{Max}	Min/Max voltage angle (rad)
$E_{es}^{ES,\min}$/ $E_{es}^{ES,\max}$	Min/Max energy level of ESs (kWh)
$E_{es}^{ES,Initial}$	Initial energy level of ESs (kWh)
$E_{hs}^{HS,\min}$/ $E_{hs}^{HS,\max}$	Min/Max energy level of HSs (kWh)
$E_{ip}^{S1-S6,\min}$/ $E_{ip}^{S1-S6,\max}$	Min/Max storage number of industrial materials (item)
$E_{ip}^{S1-S6,Initial}$	Initial number of industrial materials (item)
$E_{ev}^{EV,\min}$/ $E_{ev}^{EV,\max}$	Min/Max energy level of EVs (kWh)
$E_{ev}^{Departure,\min}$/ $E_{ev}^{Departure,\max}$	Min/Max energy level of EVs at departure time (kWh)
f_l^S	Electric line capacity (kVA)
φ_i	Bus number
$G_{i,t}^{Demand}$	Gas demand (m^3)
$G_t^{UG,Normal}$	Gas exchange with station in normal condition (m^3)
$G^{UG,\max}$	Max gas exchange rate with station (m^3)
$H2_{hs,t}^{Ch,\max}$/ $H2_{hs,t}^{Dis,\max}$	Max charging/discharging rate by HSs (kg)
$H2_{hu,t}^{Customers,Normal}$	Hydrogen consumption of P2H units at normal condition (kg)
$H_{ip}^{GB,\max}$	GB capacity (kW)
$H_{ip,t}^{EH,\max}$	EH capacity (kW)
$I_{l,t}^{Fail}$	Status of fault lines
$I_{ev,t}^{Parking}$	Status EVs at Charging Stations
IR_t	Sun irradiance (kW/m^2)

(*continued on next column*)

(*continued*)

$\lambda_{ip,t}^{P,Service}$/ $\lambda_{ip,t}^{Q,Service}$/ $\lambda_{ip,t}^{G,Service}$	Prices of services provided by industrial parks ($/kW - $/kVAR - $/$m^3$)
$\lambda_{hu,t}^{H2,Service}$	Prices of services provided by P2H units ($/kg)
$\lambda_{cs,t}^{P,Service}$/ $\lambda_{cs,t}^{Q,Service}$	Prices of services provided by charging stations ($/kW - $/kVAR)
	Production level of industrial parks at normal condition (item)
P_s^{Rate}/ P_w^{Rate}	Power rate of SU/WU (kW)
$P_{i,t}^{Demand}$/ $Q_{i,t}^{Demand}$	Electricity demand (kW/kVAR)
$P^{UG,\max}$	Max exchange rate with upstream grid (kW)
$P_t^{UG,Normal}$/ $Q_t^{UG,Normal}$	Exchange rate with upstream grid at normal condition (kW-kVAR)
$P_i^{Node,\min}$/ $P_i^{Node,\max}$	Min/Max node pressure (pa)
$P_g^{DU,\min}$/ $P_g^{DU,\max}$	Min/Max active power generation rate of DUs (kW)
$P_{es}^{Ch,\max}$/ $P_{es}^{Dis,\max}$	Max charging/discharging rate of ESs (kW)
$P_{ev,t}^{Ch,\max}$/ $P_{ev,t}^{Ch,\max}$	Max charging/discharging rate of EVs (kW)
$P_{(\cdots)}^{CHP}$/ $H_{(\cdots)}^{CHP}$	Marginal operation points of CHP (kW)
$P_{ip,t}^{Exch,Normal}$/ $Q_{ip,t}^{Exch,Normal}$/ $G_{ip,t}^{Exch,Normal}$	Energy exchanges by industrial parks at normal condition (kW/kVAR/m^3)
$P_{cs,t}^{Charger,Normal}$	Charging station demand at normal condition (kW)
$Q_g^{DU,\min}$/ $Q_g^{DU,\max}$	Min/Max reactive power generation rate of DUs (kW)
$Q_{ip}^{CB,\min}$/ $Q_{ip}^{CB,\max}$	Min/Max reactive power generation rate by CBs (kVAR)
$\pi_t^{P,Price}$/ $\pi_t^{Q,Price}$	Electricity prices ($/kW - $/KVAR)
$\pi_t^{G,Price}$	Gas price ($/$m^3$)
π_i^{LS}	Load shedding penalty ($/kW)
$R_{ip/cs/hu}^{(\cdots),Primal}$/ $R_{ip/cs/hu}^{(\cdots),Dual}$	Primal/Dual residuals
$\rho_{ip/cs/hu}^{(\cdots),r}$	Penalty factor of smart prosumers
S_{ip}^{CHP}	Discrete scaling of CHP (kw)
$S_{cs,t}^{Charger}$	Charger capacity (kVA)
$V_i^{\min}$/ $V_i^{\max}$	Min/Max voltage magnitude (p.u)
V_t	Wind speed (m/s)
$W^{(\cdots),T(\cdots)}$	Weight factor of materials in production process
$\xi_{i,l}$	Flow direction map
χ_i	Reactive consumption factor (kVAR/kW)
$\prod_l^D$/ $\prod_l^S$	Destination/Start points of travel paths

Variables

$\Delta p_{cs,t}^{Charger}$	Changes in charging station demand (kW)
$\Delta m5_{ip,t}^{Product}$	Changes in production process of industrial parks (item)
$\Delta h2_{hu,t}^{Customers}$	Changes in hydrogen demand of P2H units (kg)
$\delta_{i,t}^{Bus}$/ $\delta_{j,t}^{Bus}$	Voltage angle (rad)
$e_{es,t}^{ES}$/ $e_{hs,t}^{HS}$	Energy level of ESs/HSs (kWh)
$e_{ip,t}^{S(\cdots)}$	Number of items stores in warehouse (item)
$e_{ev,t}^{EV}$	Energy level of EVs (kWh)
$f_{l,t}^P$/ $f_{l,t}^Q$	Power flow of electric lines (kW/kVAR)
$f_{l,t}^G$	Gas flow (m^3)
$g_t^{UG,Services}$	Services provided by gas station (m^3)
g_t^{UG}	Gas exchange with station (m^3)
$g_{g,t}^{DU}$	Gas consumption of DUs (m^3)
$g_{ip,t}^{Exch}$	Services provided by industrial parks (m^3)
$g_{ip,t}^{CHP}$	Gas consumption of CHPs (m^3)
$g_{ip,t}^{GB}$/ $h_{ip,t}^{GB}$	Operation points of GB (m3/kW)
$g_{ip,t}^{GS,Ch}$/ $g_{ip,t}^{GS,Dis}$	Charging/Discharging of GSs (m^3)
$h2_{hu,t}^{Service}$	Services provided by P2H units (kg)
$h2_{hs,t}^{Ch}$/ $h2_{hs,t}^{Dis}$	Charging/Discharging of HSs (kg)
$h2_{hu,t}^{Customers}$	Hydrogen demand of P2H units (kg)
$h2_{hu,t}^{EL}$	Hydrogen generated by Electrolyzer (kg)
$h_{ip,t}^{TS,Ch}$/ $h_{ip,t}^{TS,Dis}$	Charging/Discharging of TSs (kg)
$m(\cdots)_{ip,t}^{T(\cdots)}$	Material usage in production process (item)
$m5_{ip,t}^{Product}$	Final material in production process (item)
$p_t^{UG,Services}$/ $q_t^{UG,Services}$	Service provided by upstream grid (kW/kVAR)
$p_{ip,t}^{Service}$/ $q_{ip,t}^{Service}$/ $g_{ip,t}^{Service}$	Service provided by industrial parks (kW/kVAR/m^3)
$p_{cs,t}^{Service}$/ $q_{cs,t}^{Service}$	Service provided by charging stations (kW/kVAR)
$p_{i,t}^{LS}$	Load shedding (kW)
$p_{l,t}^{Loss}$	Power loss (kW)

(*continued on next page*)

(*continued*)

p_t^{UG} / q_t^{UG}	Energy exchanges with upstream grid (kW/kVAR)
$p_{g,t}^{DU}$ / $q_{g,t}^{DU}$	Energy production by DUs (kW/kVAR)
$P_{w,t}^{WU}$ / $q_{w,t}^{WU}$	Energy production by WUs (kW/kVAR)
$P_{s,t}^{SU}$ / $q_{s,t}^{SU}$	Energy production by SUs (kW/kVAR)
$p_{es,t}^{Ch}$ / $p_{es,t}^{Dis}$	Charging/Discharging of ESs (kW)
$p_{ip,t}^{Exch}$ / $q_{ip,t}^{Exch}$	Energy exchanges of industrial parks (kW/kVAR)
$p_{cs,t}^{Exch}$ / $q_{cs,t}^{Exch}$	Energy exchanges of charging stations (kW/kVAR)
$p_{i,t}^{Node}$	Gas pressure (pa)
$p_{gs,t}^{Ch}$ / $p_{gs,t}^{Dis}$	Charging/Discharging of GSs (m^3)
$p_{hs,t}^{FC}$	Power production by FC (kW)
$p_{ip,t}^{CHP}$ / $h_{ip,t}^{CHP}$	Operation points of CHP (kW)
$p_{ip,t}^{EH}$ / $h_{ip,t}^{EH}$	Operation points of EHs (kW)
$p_{ip,t}^{(\cdots)\to(\cdots)}$ / $h_{ip,t}^{(\cdots)\to(\cdots)}$ / $g_{ip,t}^{(\cdots)\to(\cdots)}$	Internal energy flows of industrial parks (kW/kW/m^3)
$p_{ip,t}^{T(\cdots)}$ / $h_{ip,t}^{T(\cdots)}$ / $g_{ip,t}^{T(\cdots)}$	Energy consumption in production process (kW/kW/m^3)
$p_{ev,t}^{Ch}$ / $p_{ev,t}^{Dis}$	Charging/Discharging of EVs (m^3)
$p_{cs,t}^{Charger}$ / $q_{cs,t}^{Charger}$	Charging station demand (kW)
$q_{ip,t}^{CB}$	Reactive power generation by CBs (kVAR)
$q_{ip,t}^{T1-T6}$	Reactive power consumption in production process (kVAR)
$v_{i,t}^{Bus}$ / $v_{j,t}^{Bus}$	Voltage magnitude (p.u)
Binary Variables	
$i_{l,t}^{DFR}$	Status of active electric lines
$i_{i,j,t}^{Parent}$ / $i_{j,i,t}^{Parent}$	Status of parent nodes in electric lines
$i_{l,k,t}^{C}$	Status of compressor operation point
$i_{es,t}^{Ch}$ / $i_{es,t}^{Dis}$	Status of charging/discharging of ESs
$i_{hs,l,t}^{Arc}$	Status of travel paths
$i_{hs,i,t}^{Location}$	Status of HSs' location
$i_{ip,t}^{Area\ 1}$ / $i_{ip,t}^{Area\ 2}$	Status of CHP's working zone
$i_{ip,t}^{CHP}$	Status of CHP
$\alpha_{ip,t,n}^{CHP}$	Status of discrete operation point of CHP
$i_{ev,t}^{Ch}$ / $i_{ev,t}^{Dis}$	Status of charging/discharging of EVs

1. Introduction

1.1. Background and motivation

In the evolving landscape of modern energy systems, the integration of electricity and gas networks is becoming increasingly sophisticated, necessitating advanced strategies for reliability and efficiency [1]. Self-healing mechanisms in these coordinated networks play a pivotal role in ensuring uninterrupted energy supply and minimizing downtime. These mechanisms involve the automatic detection and isolation of faults, as well as the restoration of services without human intervention [2]. A key component of this self-healing capability is the role of flexible smart prosumers—entities that both consume and produce energy. Examples of these prosumers include industrial parks, electric vehicle (EV) parking lots, and P2H units. These prosumers contribute to the resilience and adaptability of energy networks through their inherent flexibility and ability to dynamically adjust their energy consumption and production in response to real-time network conditions [3,4].

Incorporating these flexible smart prosumers into the coordinated electricity and gas networks enhances the networks' ability to self-heal by providing additional resources for balancing and stabilizing energy supply and demand [5]. Their real-time responsiveness and adaptive capabilities are integral to modern self-healing strategies, ensuring that energy networks can quickly recover from disruptions and maintain reliable service for consumers. The synergy between advanced digital technologies, such as smart sensors and communication systems, and the flexible operations of smart prosumers, marks a significant advancement in the management and optimization of integrated energy systems [6,7]. One critical aspect that requires special attention is the privacy of prosumers, which is of paramount importance to them [8]. Therefore, new self-healing structures should be designed to protect prosumer privacy while maximizing the utilization of their flexible capacities.

The challenges outlined have inspired the authors to develop a comprehensive optimization mechanism aimed at enhancing the self-healing capabilities of coordinated electricity and gas networks. This mechanism enables the system operator to utilize all flexible capacities available from smart prosumers during emergency situations. The model employs a distributed approach to optimize the participation of all stakeholders, ensuring privacy and minimal information sharing.

1.2. Literature review

Recently, numerous researchers have introduced innovative strategies for the self-healing planning of electricity and gas networks. In this light [9], proposes a three-stage self-healing strategy to enhance distribution network resilience during natural disasters. It combines repair crew planning and black start resources for power and gas systems. The system is divided into microgrids, restored concurrently, and utilizes topology refurbishment, microgrid islanding, and energy storage. Uncertainties are managed with stochastic methods. This strategy minimizes downtime and speeds up restoration [10]. presents a self-healing model for distribution networks that integrates gas and electrical systems, using micro-turbines, Energy Storages (ESs), and Combined Heat and Power (CHP) units. It optimizes generation to minimize costs and reconfigures the network during faults to maintain constraints and minimize load isolation. The model, tested on a six-microgrid and 44-node system, demonstrates effective generation and demand response management [11]. provides a framework for optimal planning of electrical, heating, and cooling distributed energy resources, incorporating smart buildings under normal and shock conditions. It highlights the impact of smart buildings on energy system planning and utilizes a four-stage optimization process with a self-healing performance index. Applied to the 123-bus IEEE test system, the framework reduced system costs by 49.92 % and energy not supplied costs by 93.64 % [12]. presents a self-healing model to enhance the resilience of integrated electricity and gas networks with industrial, commercial, and residential hubs. Combining long-term system hardening and a bi-level real-time operation model, hubs optimize their schedules and coordinate with the distribution system operator, who adjusts network planning, including feeder reconfiguration and deploying mobile resources. Tested on a 69-bus electricity and 14-node gas network, the model reduces schedule deviations and forced load shedding.

Over the past years, many studies have concentrated on deploying mobile emergency units during emergency conditions to enhance system resilience [13]. presents a two-stage model to enhance distribution network resilience. The first stage coordinates investments in line hardening, distributed generators, mobile emergency generators, and switches to minimize costs. The second stage minimizes expected operational costs across scenarios. Testing on the IEEE 33-bus system using Typhoon Mangkhut data demonstrates that mobile unit allocation significantly reduce post-event costs and improve network resilience [14]. addresses the resilience-driven dispatch problem of mobile power sources and repair crews through a decentralized framework. By implementing a hierarchical multi-agent reinforcement learning method, the study introduces a two-level framework that switches decision-making between power and transport networks at a high level and computes continuous planning and discrete routing decisions at a low level. An embedded function encapsulating system dynamics is utilized to enhance learning stability and scalability. The proposed method demonstrates its effectiveness in load restoration through case studies on IEEE 33-bus and 69-bus power networks [15]. proposes a three-stage hierarchical model to improve microgrid resilience. The first stage involves proactive measures for windstorm readiness. The second stage optimizes generation planning, mobile unit allocation, and distribution feeder reconfiguration to cut operating costs. The final stage allocates repair crews to minimize load shedding. Case studies on a 118-bus network show significant load shedding reductions and a 3.47

Table 1
Comparison with recent state-of-the-art models.

Paper	System Studied		Automatic Switching	Emergency Service Providers			Load Priority	Mobile Units	Coordination Framework
	Power	Gas		Industrial Parks	Charging Stations	P2H Units			
[34]	✓	×	✓	×	×	×	✓	✓	Centralized
[35]	✓	×	×	×	×	×	×	×	Hierarchical
[36]	✓	×	✓	×	×	×	×	×	Distributed
[37]	✓	×	✓	×	×	×	✓	✓	Centralized
[33]	✓	×	✓	×	×	×	×	×	Distributed
[38]	✓	×	✓	×	×	×	✓	✓	Centralized
[30]	✓	×	✓	×	×	×	×	×	Distributed
[39]	✓	×	×	×	×	×	✓	×	Centralized
[40]	✓	×	×	×	×	×	✓	✓	Hierarchical
[41]	✓	×	✓	×	×	×	✓	×	Distributed
[31]	✓	✓	×	×	×	✓	×	×	Distributed
[42]	✓	×	×	×	×	×	×	×	Centralized
[32]	✓	×	×	×	×	×	✓	✓	Distributed
[43]	✓	×	×	×	×	×	×	×	Hierarchical
[44]	✓	×	×	×	×	×	✓	×	Hierarchical
This Paper	✓	✓	✓	✓	✓	✓	✓	✓	Distributed

% increase in the resilience index through proactive actions, mobile unit allocation and information sharing among microgrids [16]. introduces an adaptive LinDistflow model to improve microgrid resilience in power distribution systems by using a single commodity flow model, simplifying power flow calculations. This approach supports dynamic MG formation and large-scale deployment of mobile energy resources. Formulated as a mixed-integer nonlinear programming problem, it enhances computational performance. Testing on IEEE 37-Node, 123-Node, and 8500-Node Test Feeders shows that mobile unit's deployment significantly improves resilient load restoration.

Recently, many researchers have been focusing on the crucial role of smart prosumers in enhancing the resilience of modern power systems by enabling bidirectional energy transactions and supporting efficient energy management and recovery strategies [17]. introduces a two-stage self-healing model for renewable-based distribution systems under emergency conditions. The model includes smart prosumers like internet data centers, charging stations, and P2H units to enhance system flexibility. Implementation on the modified IEEE-69 bus system demonstrated significant improvements, with critical load recovery enhanced by up to 87.61 % and load shedding reduced by 7.86 %, alongside a cost reduction of 3.77 % [18]. examines the role of smart prosumers in enhancing resilience in power systems and buildings. It proposes a comprehensive methodology to evaluate electrical resilience, integrating infrastructure vulnerability, supply continuity, and voltage service quality. Applied to a university building with smart metering, the method demonstrated effective resilience assessment, suggesting its applicability to microgrids and low-voltage networks, and addressing gaps in current strategies [19]. explores enhancing power system resilience via a microgrid-centric recovery strategy using Internet-of-things (IoT), blockchain, and smart contracts for peer-to-peer energy sharing among smart prosumers. The method addresses resource allocation and demand variability, improving power recovery. Validation with university grid data shows significant improvements in resilience index, demonstrating the strategy's effectiveness [20]. reviews the integration of smart prosumers into the internet of energy and virtual power plants (VPPs). It highlights control, management, and optimization strategies for prosumers and distributed energy resources (DERs), emphasizing bidirectional peer-to-peer energy transactions. The study underscores the shift from traditional grids to resilient, prosumer-driven energy systems. In Ref. [21], a feasibility study is presented to evaluate power smoothing methods for a photovoltaic-hydrokinetic hybrid system, addressing power fluctuations from renewable intermittency. The study employs a hybrid energy storage system with supercapacitors and lithium-ion batteries, analyzing three algorithms based on technical and economic performance. The *Enhanced Linear Exponential Smoothing Method* proved effective in reducing energy costs and stabilizing voltage at the point of common coupling (PCC). Sensitivity analysis also showed that battery capacity and supercapacitor sizing significantly impact power smoothing effectiveness.

Efficient energy management and optimization in modern power systems require advanced strategies for forecasting, resource integration, and system stability. Techniques for demand-side energy management in residential heating [22] and short-term forecasting for photovoltaic power and load prediction [23,24] enhance the predictability and reliability of distributed energy resources. Moreover, impedance measurement methods for grid-connected converters [25,26] contribute to improved stability and control of distributed generation units. Integrating risk-based operations of electric vehicles in microgrids [27], alongside innovative energy storage solutions like supercritical Brayton cycles for solar power [28] and gravity-based storage technologies [29], supports resilient and efficient decentralized energy networks.

In recent years, researchers have increasingly focused on the impact of different versions of the ADMM algorithm on optimizing self-healing models in modern power systems, emphasizing their strengths in maintaining stakeholder privacy while guaranteeing global optimal solutions and enhancing operational efficiency. For instance, the authors of [4] introduce a novel bi-level strategy for enhancing smart grid self-healing using the ADMM algorithm. By coordinating Hydrogen Refueling Stations, Electric Vehicle Charging Stations, and energy hubs, the approach optimizes prosumer contributions to improve reliability and reduce downtime. Implemented on a 118-node system, the method achieved a 32.04 % reduction in Forced Load Shedding and a 17.48 % decrease in self-healing costs, demonstrating the effectiveness of smart prosumer integration [30]. presents a service restoration scheme using the ADMM algorithm to enhance the resilience of active distribution networks. By optimizing switching sequences, distributed generation, and controllable loads, the method significantly reduces computational complexity and time, demonstrating effectiveness on multiple test systems [31]. proposes a novel resilient operating strategy for the integrated electricity-natural gas system using hydrogen-enriched compressed natural gas during emergencies. The model optimizes hydrogen and methane injection to ensure gas quality and turbine safety, solved using an alternating optimization-integrated ADMM algorithm. Case studies on test systems demonstrate the strategy's effectiveness in enhancing energy crisis resistance [32]. introduces a novel coordination method for integrating repair and restoration of coupled transmission and distribution systems using repair crews and mobile emergency generators. Employing a four-stage parallel restoration model and ADMM-based decentralized coordination, the method addresses non-convexity with the alternating optimization procedure. Validated on small and large-scale systems, the approach significantly

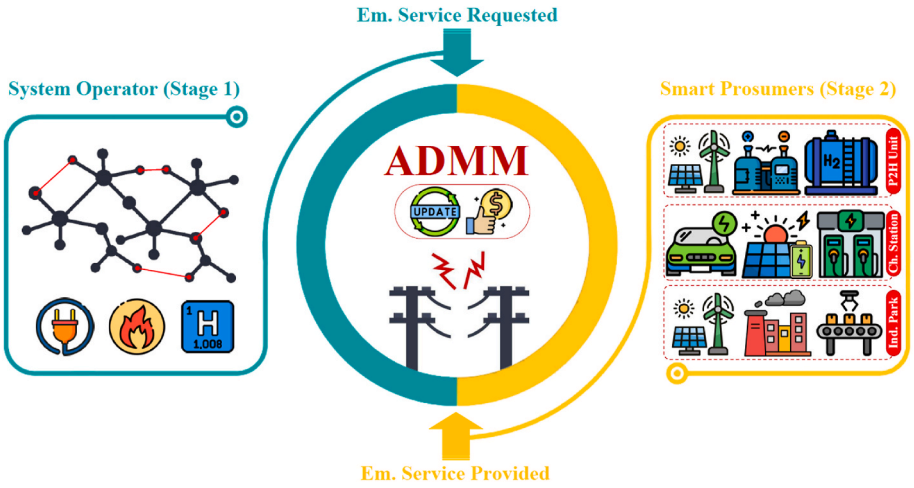

Fig. 1. The architecture of the proposed two-stage self-healing mechanism.

enhances load recovery during post-disaster repair [33]. presents a coordinated reconfiguration strategy for load restoration in integrated electric and heating systems using soft open points to enhance resilience after natural disasters. The adaptive ADMM algorithm divides the problem into distribution systems and soft open points subproblems, maintaining privacy while optimizing soft open point and valve operations. Case studies show that this strategy increases resilience metrics by 9.6 % compared to distribution system reconfiguration alone, demonstrating effective fault isolation and load restoration.

1.3. Research gap and contributions

Table 1 presents a comparison between the proposed model and recent studies in the literature. The analysis reveals that the majority of existing research relies on centralized optimization approaches for managing the operation of electricity and gas networks during emergency conditions. However, in modern power systems influenced by smart prosumers, centralized decision-making by a single entity is unrealistic. Although some studies have utilized distributed optimization techniques such as ADMM to preserve the privacy of prosumers, these algorithms often require a significant amount of time to converge. This delays the rapid coordination between users and prosumers needed for self-healing during emergencies. Therefore, there is a research gap in upgrading ADMM algorithms to ensure quick coordination between prosumers and the system operator in self-healing structures.

Furthermore, recent research emphasizes the necessity of designing new self-healing structures to fully utilize the capacities of smart prosumers in emergency situations. These prosumers have flexible electrical, gas, and hydrogen capacities that can be unlocked and provided to the system operator during emergencies through an effective optimization mechanism. This underscores the importance of developing new optimization models that maximize the capacities of smart prosumers under emergencies while maintaining the privacy of all parties involved. Additionally, the literature review reveals that no previous studies have investigated the impact of simultaneous participation by industrial parks, charging stations, and P2H units, combined with automatic switching and the deployment of fuel cell-equipped trucks, on enhancing the quality of self-healing.

To address the aforementioned research gaps, the authors of this paper propose a two-stage optimization mechanism for planning the self-healing of coordinated electricity and gas networks. This mechanism enables the system operator to leverage options such as automatic switching, fuel cell-equipped trucks, and the capacities of smart prosumers in self-healing planning. The proposed mechanism employs an augmented ADMM algorithm to coordinate the system operator with prosumers, achieving high convergence speed while preserving the privacy of all stakeholders. Below is a summary of the innovations presented in this paper:

- **Two-Stage Optimization Mechanism:** This mechanism enhances self-healing planning for coordinated electricity and gas networks by unlocking the flexible capacities of smart prosumers (industrial parks, P2H units, charging stations), rerouting power flow through feeder reconfiguration, and injecting power via fuel cell-equipped trucks at critical network points, significantly reducing operational costs and load shedding during emergencies.
- **Space-Time Network Model:** Integrates electrical and transportation constraints to optimize the dispatch of fuel cell-equipped trucks, enabling them to receive hydrogen from P2H units, convert it to electricity, and inject it at strategic points, thereby enhancing load supply to high-priority consumers and improving the resilience index.
- **Augmented ADMM Algorithm:** Ensures decentralized coordination between the system operator and smart prosumers with minimal information exchange, achieving faster convergence compared to the original ADMM by dynamically updating penalty coefficients using a logarithmic term, while maintaining global optimality.

2. Model outline

Fig. 1 depicts the architecture of the two-stage mechanism proposed for self-healing planning of coordinated electricity and gas networks in emergency situations. This structure is designed to maximize the participation of smart prosumers under emergency situations in electricity and gas networks. In the proposed concept, the operational planning of both electricity and gas networks is coordinated with a 30-min step by a single operator. This operator is also responsible for planning the self-healing of these networks in the event of an error.

At the first stage, the system operator handles the operational planning of electricity and gas networks, feeder reconfiguration, and the distribution of fuel cell-equipped trucks. At the end of this stage, the operator determines the emergency capacities of electricity, gas, and hydrogen required for self-healing of the system and sends these requirements as separate pulses to smart prosumers, including industrial parks, P2H units, and charging stations. These pulses include the requested capacity and the exchange price. The operator considers all security constraints of the electricity and gas networks and uses a space-time network to optimally distribute fuel cell-equipped trucks, combining electrical and transportation constraints.

At the second stage, smart prosumers are modeled to provide active

and reactive power, gas, and hydrogen emergency services to the system operator. They adjust their internal programming to provide these services according to the emergency pulses received from the system operator.

Smart prosumers adjust their previous planning, originally designed for normal operating conditions, to offer their available flexible capacities to the system operator. In this light, industrial parks can shift some tasks to periods after the emergency and change the planning of their generation and storage units. Charging stations can switch to emergency mode, charging their covered vehicles up to 75 % of their battery capacity instead of 95 %. P2H units can provide hydrogen stored in their tanks to the system operator. This way, electric, gas, and hydrogen capacities are made available for the system operator.

To respect the privacy of all stakeholders, an augmented ADMM algorithm has been introduced that ensures the convergence of optimization problems at both stages with minimal information sharing. This algorithm operates iteratively, with the only information exchanged between the first and second stage being the amount of emergency services and their exchange price. This approach guarantees the convergence of optimization at the global optimal point.

3. Mathematical modeling of the proposed two-stage mechanism

In this section, the mathematical formulation of the proposed two-stage self-healing mechanism is designed as a Mixed-Integer Quadratically Constrained Programming (MIQCP) problem. It should be noted that in the presented mathematical model, uppercase letters indicate parameters, whereas lowercase letters refer to variables.

3.1. Stage 1 (system operator)

The first stage of the proposed mechanism addresses the role of the system operator, who is responsible for planning the electricity and gas networks, reconfiguring the feeder, and dispatching fuel cell-equipped trucks under emergency conditions. The objective function of the first stage, presented in (1), aims to minimize the costs of purchasing emergency services in the event of an error. The first to fourth terms of this function represent the costs of purchasing services from the upstream grid, industrial parks, P2H units, and charging stations, respectively. The fifth term models the penalty incurred due to load shedding. Terms with absolutes are linearized using the Big-M method.

$$\min of^{SO} = \sum_{t} \left(\begin{array}{l} p_t^{UG,Services}\pi_t^{P,Price} + \left|q_t^{UG,Services}\right|\pi_t^{Q,Price} + g_t^{UG,Services}\pi_t^{G,Price} \\ +\sum_{ip}\left(p_{ip,t}^{Service}\lambda_{ip,t}^{P,Service} + \left|q_{ip,t}^{Service}\right|\lambda_{ip,t}^{Q,Service} + g_{ip,t}^{Service}\lambda_{ip,t}^{G,Service}\right) \\ +\sum_{hu}\left(h2_{hu,t}^{Service}\lambda_{hu,t}^{H2,Service}\right) + \sum_{cs}\left(p_{cs,t}^{Service}\lambda_{cs,t}^{P,Service} + \left|q_{cs,t}^{Service}\right|\lambda_{cs,t}^{Q,Service}\right) \\ +\sum_{i}\left(p_{i,t}^{LS}\pi_i^{LS}\right) \end{array} \right) \quad (1)$$

- **Power Flow and Feeder Reconfiguration Constraints**

Equations (1a)-(1n) represent a linearized model for the AC power flow program [45]. In this regard, (1a) and (1b) define the upper and lower bounds for active power flow ($f_{l,t}^{P}$) on the transmission line, considering bus voltage angles ($v_{i,t}^{Bus}$/ $v_{j,t}^{Bus}$) and magnitudes ($\delta_{i,t}^{Bus}$/ $\delta_{j,t}^{Bus}$), line susceptance (B_l) and conductance (G_l), and an indicator for line status during feeder reconfiguration ($i_{l,t}^{DFR}$). (1c) and (1d) also define the same constraints for reactive power flow. The Big M method is used in Eqs. (1a)-(1d) to exclude inactive lines from consideration. (1e) calculates the power loss ($p_{l,t}^{Loss}$) on a transmission line based on its resistance (R_l) and the squared magnitudes of active and reactive power flows. The quadratic terms are linearized using the piecewise method. (1f) sets the limits for bus voltage magnitudes, and (1g) defines the permissible range for bus voltage angles. (1h) ensures that the apparent power flow on a transmission line does not exceed a specified limit, modulated by its active or inactive status. (1i) represents the nodal active power balance equation, taking into account power from various sources, load demand, load shedding, and exchanges with smart prosumers. The term $p_{hs,t}^{FC} i_{hs,i,t}^{Location}$, which is the product of the binary variable $i_{hs,i,t}^{Location}$ and the continuous variable $p_{hs,t}^{FC}$, is linearized using the Big-M method. (1j) outlines the nodal reactive power balance, considering contributions from various sources, reactive power demand, and exchanges with smart prosumers. (1k) limits the load shedding at a bus to be less than or equal to the power demand at that bus. (1l) imposes limits on the power exchange with the upstream grid. (1m) and (1n) define the active ($p_t^{UG,Services}$) and reactive power services ($q_t^{UG,Services}$) provided by the upstream grid. These are calculated as the difference between the power exchange during the emergency period and the power exchange scheduled for the normal operating condition. (1o) calculates the resilience index as the ratio of total actual demand served to the total demand, expressed as a percentage, indicating the system's ability to meet demand. ω^{Normal} and $\omega^{Critical}$ are weighted coefficient of normal and critical loads, respectively.

$$f_{l,t}^{P} \le B_l\left(\delta_{i,t}^{Bus} - \delta_{j,t}^{Bus}\right) + G_l\left(v_{i,t}^{Bus} - v_{j,t}^{Bus}\right) + \left(1 - i_{l,t}^{DFR}\right)M \quad (1a)$$

$$f_{l,t}^{P} \ge B_l\left(\delta_{i,t}^{Bus} - \delta_{j,t}^{Bus}\right) + G_l\left(v_{i,t}^{Bus} - v_{j,t}^{Bus}\right) - \left(1 - i_{l,t}^{DFR}\right)M \quad (1b)$$

$$f_{l,t}^{Q} \le G_l\left(\delta_{j,t}^{Bus} - \delta_{i,t}^{Bus}\right) + B_l\left(v_{i,t}^{Bus} - v_{j,t}^{Bus}\right) + \left(1 - i_{l,t}\right)M \quad (1c)$$

$$f_{l,t}^{Q} \ge G_l\left(\delta_{j,t}^{Bus} - \delta_{i,t}^{Bus}\right) + B_l\left(v_{i,t}^{Bus} - v_{j,t}^{Bus}\right) - \left(1 - i_{l,t}\right)M \quad (1d)$$

$$p_{l,t}^{Loss} = R_l\left[\left(f_{l,t}^{P}\right)^2 + \left(f_{l,t}^{Q}\right)^2\right] \quad (1e)$$

$$V_i^{\min} \le v_{i,t}^{Bus} \le V_i^{\max} \quad (1f)$$

$$\delta_i^{Min} \le \delta_{i,t}^{Bus} \le \delta_i^{Max} \tag{1g}$$

$$\left(f_{l,t}^{P}\right)^2 + \left(f_{l,t}^{Q}\right)^2 \le \left(f_l^{S}\right)^2 i_{l,t}^{DFR} \tag{1h}$$

$$p_t^{UG}\big|_{i=1} + \sum_{g\in\Lambda_i^g} p_{g,t}^{DU} + \sum_{w\in\Lambda_i^w} P_{w,t}^{WU} + \sum_{s\in\Lambda_i^s} P_{s,t}^{SU} + \sum_{es\in\Lambda_i^{es}} \left(p_{es,t}^{Dis} - p_{es,t}^{Ch}\right) + \sum_{hs} \left(p_{hs,t}^{FC} i_{hs,i,t}^{Location}\right) = P_{i,t}^{Demand} - p_{i,t}^{LS} + \sum_{ip\in\Lambda_i^{ip}} p_{ip,t}^{Exch} + \sum_{cs\in\Lambda_i^{cs}} p_{cs,t}^{Exch} + \sum_{l\in\Lambda_i^{l}} \left(\xi_{i,l} f_{l,t}^{P} + \frac{p_{l,t}^{Loss}}{2}\right) \tag{1i}$$

$$q_t^{UG}\big|_{i=1} + \sum_{g\in\Lambda_i^g} q_{g,t}^{DU} + \sum_{w\in\Lambda_i^w} q_{w,t}^{WU} + \sum_{s\in\Lambda_i^s} q_{s,t}^{SU} = Q_{i,t}^{Demand} - \chi_i p_{i,t}^{LS} + \sum_{ip\in\Lambda_i^{ip}} q_{ip,t}^{Exch} + \sum_{cs\in\Lambda_i^{cs}} q_{cs,t}^{Exch} + \sum_{l\in\Lambda_i^{l}} \left(\xi_{i,l} f_{l,t}^{Q}\right) \tag{1j}$$

$$p_{i,t}^{LS} \le P_{i,t}^{Demand} \tag{1k}$$

$$-P^{UG,\max} \le p_t^{UG} \le P^{UG,\max} \tag{1l}$$

$$p_t^{UG,Services} = p_t^{UG} - P_t^{UG,Normal} \tag{1m}$$

$$q_t^{UG,Services} = q_t^{UG} - Q_t^{UG,Normal} \tag{1n}$$

$$RI_t = \frac{\omega^{Normal} \sum_{i\in\Lambda_{Normal}^{i}} \left(P_{i,t}^{Demand} - p_{i,t}^{LS}\right) + \omega^{Critical} \sum_{i\in\Lambda_{Critical}^{i}} \left(P_{i,t}^{Demand} - p_{i,t}^{LS}\right)}{\omega^{Normal} \sum_{i\in\Lambda_{Normal}^{i}} P_{i,t}^{Demand} + \omega^{Critical} \sum_{i\in\Lambda_{Critical}^{i}} P_{i,t}^{Demand}} \times 100 \tag{1o}$$

Constraints (1p)-(1s) enable the system operator to carry out feeder reconfiguration. Constraint (1p) establishes the direction of power flow in the active lines that are currently in operation. The binary variable $i_{l,t}^{DFR}$ indicates whether each line is present or absent at time t. Constraint (1q) ensures that each bus can receive power from only one line. Constraint (1r) prohibits the injection of power into the slack bus. Lastly, (1s) excludes faulted lines from the feeder reconfiguration program. $I_{l,t}^{Fail}$ is a parameter with a value of 1 for faulted lines.

$$i_{i,j,t}^{Parent} + i_{j,i,t}^{Parent} = i_{l,t}^{DFR} \tag{1p}$$

$$\sum_i i_{i,j,t}^{Parent} \le 1 \tag{1q}$$

$$\sum_i i_{i,j=1,t}^{Parent} = 0 \tag{1r}$$

$$i_{l,t}^{DFR} \le 1 - I_{l,t}^{Fail} \tag{1s}$$

- **Gas Flow Constraints**

The operational constraints of the gas network are described by (2a)-(2g) [46]. Constraint (2a) regulates the nodal gas pressure levels ($p_{i,t}^{Node}$). (2b) determines the gas flow through each pipeline ($f_{l,t}^{G}$), which is linearized using a piecewise approximation for simplification. In this equation, $p_{i,t}^{Node}$ and $p_{j,t}^{Node}$ represent the pressures at the inlet and outlet of the pipeline, respectively, while C_l^2 is a constant that depends on the physical properties of the pipeline. The quadratic terms associated with the pressures are linearized using a piecewise approach. (2c) models the impact of the compressor on gas pressure, where α_k^C represents the level of pressure amplification, determined by the binary variable $i_{l,k,t}^{C}$. (2d) stipulates that only one operational mode can be selected for the compressor at any given time. (2e) ensures the nodal balance within the gas network. (2f) defines the gas services procured from the station, considering the discrepancy between emergency period purchases and those scheduled for the normal operating condition. Lastly, (2g) imposes an hourly limit on gas purchases from the station.

$$P_i^{Node,\min} \le p_{i,t}^{Node} \le P_i^{Node,\max} \tag{2a}$$

$$f_{l,t}^{G}\left|f_{l,t}^{G}\right| = C_l^2\left[\left(p_{i,t}^{Node}\right)^2 - \left(p_{j,t}^{Node}\right)^2\right] \tag{2b}$$

$$p_{j,t}^{Node} = \sum_k \left(i_{l,k,t}^{C} \alpha_k^{C}\right) p_{i,t}^{Node} \tag{2c}$$

$$\sum_k i_{l,k,t}^{C} = 1 \tag{2d}$$

$$g_t^{UG}\big|_{i=1} + \sum_{gs\in\Lambda_i^{gs}} \left(p_{gs,t}^{Dis} - p_{gs,t}^{Ch}\right) = G_{i,t}^{Demand} + \sum_{g\in\Lambda_i^g} g_{g,t}^{DU} + \sum_{ip\in\Lambda_i^{ip}} g_{ip,t}^{Exch} + \sum_{l\in\Lambda_i^{l}} \left(\xi_{i,l} f_{l,t}^{G}\right) \tag{2e}$$

$$g_t^{UG,Services} = g_t^{UG} - G_t^{UG,Normal} \tag{2f}$$

$$0 \le g_t^{UG} \le G^{UG,\max} \tag{2g}$$

- **Power Generation and Storage Units**

Equations (3a)-(3f) define the operational constraints and relationships for various power generation units in the system [47]. (3a) establishes the minimum and maximum limits for the active power generation from distributed units (DU), while (3b) sets similar constraints for the reactive power. Equation (3c) expresses the active power generation from distributed units as a function of the fuel consumption ($g_{g,t}^{DU}$), using the efficiency parameter (η_{ge}^{DU}). (3d) relates the active power generation from solar units ($P_{s,t}^{SU}$) to the irradiance rate (IR_t), incorporating the efficiency factor (η^{SU}) and standard test conditions (IR^{STC}). (3e) defines the active power generation from wind units ($P_{w,t}^{WU}$) as a piecewise function of the wind speed, with different conditions for cut-in (V_w^{ci}), rated (V_w^{r}), and cut-out speeds (V_w^{co}). Finally, (3f) provides the constraints for the reactive power generation from both solar and wind units, expressed as a function of their respective active power generation and power factor limits.

$$P_g^{DU,\min} \le p_{g,t}^{DU} \le P_g^{DU,\max} \tag{3a}$$

$$Q_g^{DU,\min} \le q_{g,t}^{DU} \le Q_g^{DU,\max} \tag{3b}$$

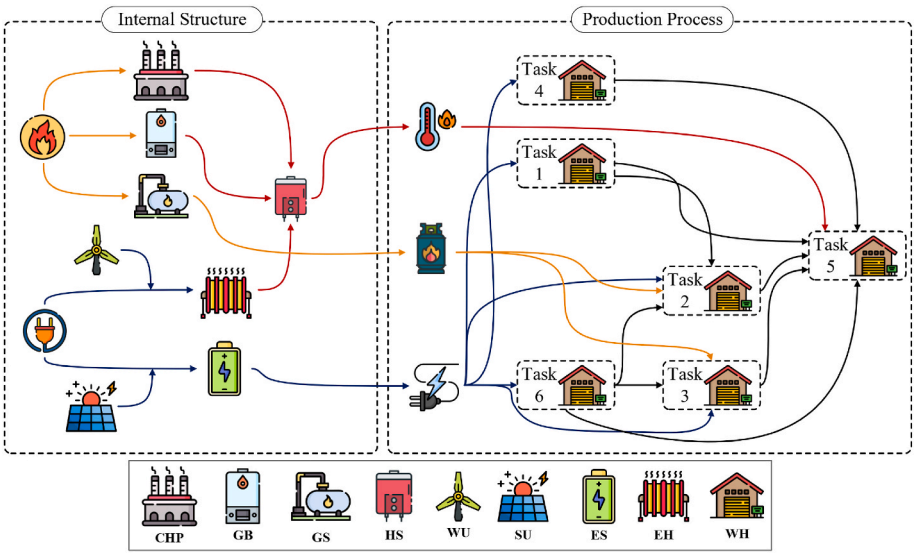

Fig. 2. The internal structure of the industrial unit under investigation.

$$p_{g,t}^{DU} = \eta_{ge}^{DU} g_{g,t}^{DU} \tag{3c}$$

$$P_{s,t}^{SU} = \eta^{SU} \frac{IR_t}{IR^{STC}} P_s^{Rate} \tag{3d}$$

$$P_{w,t}^{WU} = \begin{cases} 0, V_t < V_w^{ci} \ \ or \ \ V_t \geq V_w^{co} \\ P_w^{Rate} \dfrac{V_t - V_w^r}{V_w^{ci} - V_w^r}, V_w^{ci} \leq V_t < V_w^r \\ P_w^{Rate}, V_w^r \leq V_t < V_w^{co} \end{cases} \tag{3e}$$

$$-\frac{p_{s/w,t}^{SU/WU}\sqrt{1-(\Upsilon^{SU/WU})^2}}{\Upsilon^{WU}} \leq q_{s/w,t}^{SU/WU} \leq \frac{p_{s/w,t}^{SU/WU}\sqrt{1-(\Upsilon^{SU/WU})^2}}{\Upsilon^{SU/WU}} \tag{3f}$$

The set of equations describe the energy storage (ES) system are provided in (3g)-(3l). (3g) represents the energy balance within the storage system, considering the charging and discharging power over a time interval. (3h) sets the limits for the charging power and (3i) defines the limits for the discharging power. Charging and discharging operations are determined by the binary variables $i_{es,t}^{Ch}$ and $i_{es,t}^{Dis}$. (3j) ensures that the ES cannot charge and discharge simultaneously by limiting the sum of the charging and discharging indicators to be at most one. (3k) imposes the bounds on the energy stored in the ES, and (3l) sets the initial energy level of the ES to be at least the initial specified value.

$$e_{es,t}^{ES} = e_{es,t-1}^{ES} + \left(p_{es,t}^{Ch}\eta^{Ch} - \frac{p_{es,t}^{Dis}}{\eta^{Dis}}\right)\Delta t \tag{3g}$$

$$0 \leq p_{es,t}^{Ch} \leq P_{es}^{Ch,\max} i_{es,t}^{Ch} \tag{3h}$$

$$0 \leq p_{es,t}^{ES,Dis} \leq P_{es}^{Dis,\max} i_{es,t}^{Dis} \tag{3i}$$

$$i_{es,t}^{Ch} + i_{es,t}^{Dis} \leq 1 \tag{3j}$$

$$E_{es}^{ES,\min} \leq e_{es,t}^{ES} \leq E_{es}^{ES,\max} \tag{3k}$$

$$e_{es,t=0}^{ES} \geq E_{es}^{ES,Initial} \tag{3l}$$

- **Routing of Fuel Cell-Equipped Trucks**

A formulation based on the time-space network concept [48] is provided for modeling the routing and operational constraints of fuel cell-equipped hydrogen trucks in (4a)-(4k). These trucks are equipped with a hydrogen tank and a fuel cell. In emergencies, the system operator sends these trucks to the P2H units to load hydrogen into their Hydrogen Storage (HS). Then, the operator dispatches them to designated points to convert the hydrogen into electricity using fuel cells and inject it into the network.

(4a) defines the arc of the travel path of each truck using the binary variable $i_{hs,l,t}^{Arc}$. (4b) ensures continuity of truck movement by stating that the destination point of each truck at time t ($\prod_l^D$) must be equal to the source point at time $t+1$ ($\prod_l^S$). (4c) specifies that when trucks are dispatched, one of the arcs connected to the depot must be activated. (4d) ensures that at the end of the time horizon ($t = T$), the number of trucks returning to the depot matches the initial number of trucks at the depot. (4e) links the candidate nodes of the power grid to the endpoints of the arcs. $i_{hs,i,t}^{Location}$ is the binary variable associated with each candidate node, and φ_i is the identifier number of that node.

(4f)-(4j) models the Hydrogen Storage (HS) and fuel cell of the trucks [45]. (4f) calculates the hydrogen level in the HS at any time t ($e_{hs,t}^{HES}$), taking into account the previous time hydrogen rate ($e_{ip,t-1}^{HES}$) and the net hydrogen charged ($h2_{hs,t}^{Ch}$) or discharged ($h2_{hs,t}^{Dis}$). (4g) and (4h) impose constraints on hydrogen charging and discharging, respectively. Considering the binary variable $i_{hs,i,t}^{Location}$ in these constraints ensures that the charging of HS occurs only in buses coupled to P2H units, and its discharge takes place only in candidate buses of the electrical network. (4i) states that the HS truck charge should be equal to the service purchased from the P2H unit. (4j) shows that the hydrogen discharged from HS is converted into electricity ($P_{hs,t}^{FC}$) by the fuel cell. LHV^{H2} and η^{FC} represent the lower heating value of hydrogen and the efficiency of this equipment, respectively. (4k) enforces the upper and lower bounds on the hydrogen level in the HS.

$$\sum_l i_{hs,l,t}^{Arc} = 1 \tag{4a}$$

$$\sum_l \left(i_{hs,l,t}^{Arc} \prod_l^D\right) = \sum_l \left(i_{hs,l,t+1}^{Arc} \prod_l^S\right) \tag{4b}$$

$$\sum_l \left(i_{hs,l,t=0}^{Arc} \prod_l^S\right) = \prod^{Depot} \tag{4c}$$

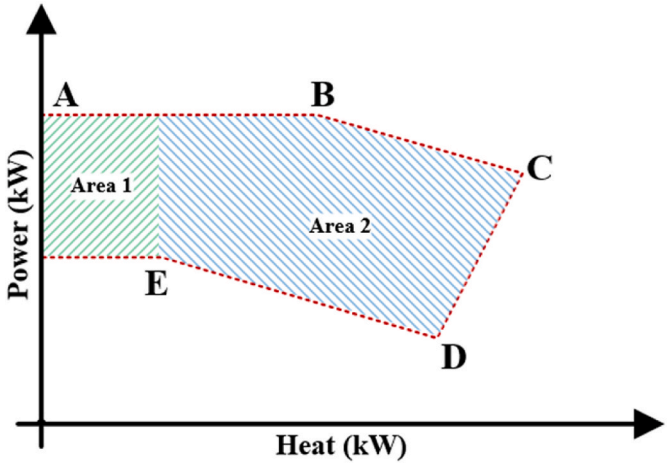

Fig. 3. Feasible operation areas of the CHP unit.

$$\sum_{l}\left(i^{Arc}_{hs,l,t=T}\prod^{D}_{l}\right)=\prod^{Depot} \tag{4d}$$

$$\sum_{i}\left(i^{Location}_{hs,i,t}\varphi_{i}\right)=\sum_{l}\left(i^{Arc}_{hs,l,t}\prod^{D}_{l}\right) \tag{4e}$$

$$e^{HS}_{hs,t}=e^{HS}_{hs,t-1}+\frac{R^{H2}T^{H2}}{V^{H2}}\left(h2^{Ch}_{hs,t}-h2^{Dis}_{hs,t}\right)\Delta t \tag{4f}$$

$$0\le h2^{Ch}_{hs,t}\le H2^{Ch,\max}_{hs,t}\sum_{i\in\Lambda^{i}_{Real}} i^{Location}_{hs,i,t} \tag{4g}$$

$$0\le h2^{Dis}_{hs,t}\le H2^{Dis,\max}_{hs,t}\sum_{i\in\Lambda^{i}_{Real}} i^{Location}_{hs,i,t} \tag{4h}$$

$$h2^{Ch}_{hs,t}=h2^{Service}_{hu,t} \tag{4i}$$

$$p^{FC}_{hs,t}=h2^{Dis}_{hs,t}LHV^{H2}\eta^{FC} \tag{4j}$$

$$E^{HS,\min}_{hs}\le e^{HS}_{hs,t}\le E^{HS,\max}_{hs} \tag{4k}$$

3.2. Stage 2 (smart prosumers)

In the second stage of the proposed mechanism, smart prosumers include industrial parks, P2H units, and charging stations are modeled. Each of these prosumers is programmed separately and decentralized, connecting to the system operator using an augmented ADMM algorithm. These prosumers can provide emergency services to the system operator in the form of active and reactive power, as well as gas and hydrogen. They deliver these services by adjusting the planning of their generation and storage components, as well as their consumptions. Note that the internal processes of the industrial park are modeled using the Energy Flow concept.

3.2.1. Industrial parks

Fig. 2 illustrates the structure of the industrial park, equipped with wind turbines, solar systems, CHP units, gas boilers, electric heaters, capacitor banks (CBs), and storage systems. It is connected to electricity and gas networks, requiring electrical, thermal, and gas energy for operation. Electricity is supplied by both the grid and local sources. Gas is supplied through the network, and heat is generated locally by the electric heating system. As per Fig. 2, Products 1, 2, 3, 4 and 6, after production, can either be used in the manufacturing processes of other products or stored in the warehouse. Product 5, which is the final product of the industrial park, can be stored in the warehouse or sold on the market.

Equation (2) presents their objective function, which is modeled to maximize the sales of emergency services to the system while considering the costs associated with changes in production levels. The first to third terms represent the exchanges of active, reactive, and gas services, respectively, while the fourth term accounts for the cost of reductions in production levels ($\Delta m5^{Product}_{ip,t}\pi^{Product}$).

$$\max of_{ip}=\sum_{t}\left(p^{Service}_{ip,t}\lambda^{P,Service}_{ip,t}+\left|q^{Service}_{ip,t}\right|\lambda^{Q,Service}_{ip,t}+g^{Service}_{ip,t}\lambda^{G,Service}_{ip,t}-\Delta m5^{Product}_{ip,t}\pi^{Product}\right) \tag{2}$$

- **Industrial Park Components**

Equations (5a)-(5k) model the operation of the CHP unit within the industrial park [49]. The CHP unit under investigation has two feasible operation areas, as shown in Fig. 3. Constraint (5a) determines the area of operation if the CHP is on. If the CHP is active in area 1, the binary variable $i^{Area\ 1}_{ip,t}$ is equal to 1, and if it is active in area 2, the binary variable $i^{Area\ 2}_{ip,t}$ is equal to 1. The binary variable $i^{CHP}_{ip,t}$ determines whether the CHP is on or off. (5b) and (5c) establish upper bounds for power ($p^{CHP}_{ip,t}$) and heat ($h^{CHP}_{ip,t}$) outputs, ensuring that these outputs are zero when the unit is off. Further, (5d)-(5i) determine the feasible operational areas for heat and power outputs in specific operational areas, incorporating conditions that activate or deactivate these ranges based on the status of the binary variables $i^{Area\ 1}_{ip,t}$ and $i^{Area\ 2}_{ip,t}$. These constraints ensure that the CHP unit operates within safe and efficient boundaries, reflecting the physical and operational limitations. (5j) determines the range of injection/absorption of reactive power of the CHP unit, considering the rate of active power. Lastly, (5k) provides a quadratic function representing the gas consumption of the CHP unit, taking into account the quadratic terms of power and heat outputs, their cross-term ($p^{CHP}_{ip,t}h^{CHP}_{ip,t}$), and a fixed value ($F$).

$$i^{Area\ 1}_{ip,t}+i^{Area\ 2}_{ip,t}=i^{CHP}_{ip,t} \tag{5a}$$

$$0\le p^{CHP}_{ip,t}\le P^{CHP}_{A}i^{CHP}_{ip,t} \tag{5b}$$

$$0\le h^{CHP}_{ip,t}\le H^{CHP}_{C}i^{CHP}_{ip,t} \tag{5c}$$

$$0\le h^{CHP}_{ip,t}-H^{CHP}_{E}\le\left(1-i^{Area\ 1}_{ip,t}\right)\left(H^{CHP}_{C}-H^{CHP}_{E}\right) \tag{5d}$$

$$0\le p^{CHP}_{ip,t}-P^{CHP}_{E}\ge\left(i^{Area\ 1}_{ip,t}-1\right)E^{CHP}_{E} \tag{5e}$$

$$0\le h^{CHP}_{ip,t}-H^{CHP}_{E}\ge\left(i^{Area\ 2}_{ip,t}-1\right)H^{CHP}_{E} \tag{5f}$$

$$p^{CHP}_{ip,t}-P^{CHP}_{D}-\frac{P^{CHP}_{D}-P^{CHP}_{E}}{H^{CHP}_{D}-H^{CHP}_{E}}\left(h^{CHP}_{ip,t}-H^{CHP}_{D}\right)\ge\left(i^{Area\ 2}_{ip,t}-1\right)\left(P^{CHP}_{D}-\frac{\left(P^{CHP}_{D}-P^{CHP}_{E}\right)\left(H^{CHP}_{D}\right)}{H^{CHP}_{D}-H^{CHP}_{E}}\right) \tag{5g}$$

$$p^{CHP}_{ip,t}-P^{CHP}_{B}-\frac{P^{CHP}_{B}-P^{CHP}_{C}}{P^{CHP}_{B}-P^{CHP}_{C}}\left(h^{CHP}_{ip,t}-H^{CHP}_{C}\right)\le\left(1-i^{Area\ 2}_{ip,t}\right)\left(P^{CHP}_{A}-P^{CHP}_{B}-\frac{\left(P^{CHP}_{B}-P^{CHP}_{C}\right)\left(H^{CHP}_{C}-H^{CHP}_{B}\right)}{H^{CHP}_{B}-H^{CHP}_{C}}\right) \tag{5h}$$

$$p^{CHP}_{ip,t}-P^{CHP}_{C}-\frac{P^{CHP}_{C}-P^{CHP}_{D}}{H^{CHP}_{C}-H^{CHP}_{D}}\left(h^{CHP}_{ip,t}-H^{CHP}_{C}\right)\ge\left(i^{Area\ 2}_{ip,t}-1\right)P^{CHP}_{C} \tag{5i}$$

$$-\gamma^{CHP}p^{CHP}_{ip,t}\le q^{CHP}_{ip,t}\le\gamma^{CHP}p^{CHP}_{ip,t} \tag{5j}$$

$$g_{ip,t}^{CHP} = A\left(p_{ip,t}^{CHP}\right)^2 + B\,p_{ip,t}^{CHP} + C\left(h_{ip,t}^{CHP}\right)^2 + D\,h_{ip,t}^{CHP} + E\,p_{ip,t}^{CHP}h_{ip,t}^{CHP} + F\,i_{ip,t}^{CHP} \tag{5k}$$

Equations (5l)-(5s) linearize the nonlinear term ($p_{ip,t}^{CHP}h_{ip,t}^{CHP}$) in (5k). Equation (5l) introduces a new variable ($ph_{ip,t}^{CHP}$) representing the product of electrical and thermal outputs. (5m)-(5o) break down the thermal output into a sum of weighted terms. To facilitate linearization, the heat output is expressed as a sum of scaled binary variables ($\alpha_{ip,t,n}^{CHP}$) in (5m), with a scaling factor (S_{ip}^{CHP}) introduced in (5n). The product of power and heat outputs is then represented in terms of these scaled variables and their sums, as shown in (5o). Equation (5p) introduces a new intermediate variable ($w_{ip,t,n}^{CHP}$) as a product of weights and heat output. Equation (5q) provides bounds for this new variable. Equation (5r) imposes additional bounds based on the weights, heat output and Big-M method. Finally, (5s) defines the product of electrical and heat outputs as a sum of the new weighted terms.

$$ph_{ip,t}^{CHP} \triangleq p_{ip,t}^{CHP}h_{ip,t}^{CHP} \tag{5l}$$

$$h_{ip,t}^{CHP} = S_{ip}^{CHP}\sum_{n}\alpha_{ip,t,n}^{CHP} \tag{5m}$$

$$S_{ip}^{CHP} = \frac{H_{ip}^{C}}{N^{CHP}} \tag{5n}$$

$$ph_{ip,t}^{CHP} \triangleq S_{ip}^{CHP}\sum_{n}\left(\alpha_{ip,t,n}^{CHP}p_{ip,t}^{CHP}\right) \tag{5o}$$

$$w_{ip,t,n}^{CHP} \triangleq \alpha_{ip,t,n}^{CHP}h_{ip,t}^{CHP} \tag{5p}$$

$$-\alpha_{ip,t,n}^{CHP}M \le w_{ip,t,n}^{CHP} \le \alpha_{ip,t,n}^{CHP}M \tag{5q}$$

$$h_{ip,t}^{CHP} - \left(1-\alpha_{ip,t,n}^{CHP}\right)M \le w_{ip,t,n}^{CHP} \le h_{ip,t}^{CHP} + \left(1-\alpha_{ip,t,n}^{CHP}\right)M \tag{5r}$$

$$ph_{ip,t}^{CHP} = S_{ip}^{CHP}\sum_{n}w_{ip,t,n}^{CHP} \tag{5s}$$

Equation (5t) presents the production function of the GB, whose heat production ($h_{ip,t}^{GB}$) depends on its gas consumption ($g_{ip,t}^{GB}$) using the efficiency factor η_{gh}^{GB}. (5u) limits the maximum heat production of the GB to its capacity ($H_{ip}^{GB,\max}$). Equation (5v) models the production function of the electric heater by considering the electricity consumption ($p_{ip,t}^{EH}$) of this component and its efficiency factor (η_{eh}^{EH}). Constraint (5w) limits the maximum heat production of this component. Equation (5x) models the exploitation range of CB inside the industrial park. This CB can be placed in both lead and lag modes, providing significant flexible capacities for reactive power emergency services.

$$h_{ip,t}^{GB} = \eta_{gh}^{GB}g_{ip,t}^{GB} \tag{5t}$$

$$h_{ip,t}^{GB} \le H_{ip}^{GB,\max} \tag{5u}$$

$$h_{ip,t}^{EH} = \eta_{eh}^{EH}p_{ip,t}^{EH} \tag{5v}$$

$$h_{ip,t}^{EH} \le H_{ip,t}^{EH,\max} \tag{5w}$$

$$Q_{ip}^{CB,\min} \le q_{ip,t}^{CB} \le Q_{ip}^{CB,\max} \tag{5x}$$

- **The Energy Flow of the Industrial Park**

Equations (6a)–(6c) respectively model the active, reactive, and gas services that can be provided in the industrial park. These services are equal to the difference between the exchanges determined for the normal operating condition and the new exchanges during the emergency period. Parameters $P_{ip,t}^{Exch,DA}$, $Q_{ip,t}^{Exch,DA}$, and $G_{ip,t}^{Exch,DA}$, which determine the exchanges for normal operation, are considered as inputs in self-healing programming. (6a)–(6c) illustrate that the values of active power ($p_{ip,t}^{Exch}$), reactive power ($q_{ip,t}^{Exch}$) and gas ($g_{ip,t}^{Exch}$) exchanges during the emergency period are determined based on the operating points of industrial park local components and load consumptions for performing daily tasks.

$$p_{ip,t}^{Service} = P_{ip,t}^{Exch,Normal} - \left(\underbrace{p_{ip,t}^{Grid\to Load} + p_{ip,t}^{Grid\to EH} + p_{ip,t}^{Grid\to ES} - p_{ip,t}^{CHP\to Grid} - p_{ip,t}^{RES\to Grid} - p_{ip,t}^{ES\to Grid}}_{p_{ip,t}^{Exch}}\right) \tag{6a}$$

$$q_{ip,t}^{Service} = Q_{ip,t}^{Exch,Normal} - \left(\underbrace{q_{ip,t}^{Grid\to Load} - q_{ip,t}^{RES\to Grid} - q_{ip,t}^{CB\to Grid}}_{q_{ip,t}^{Exch}}\right) \tag{6b}$$

$$g_{ip,t}^{Service} = G_{ip,t}^{Exch,Normal} - \left(\underbrace{g_{ip,t}^{Grid\to Load} + g_{ip,t}^{Grid\to CHP} + g_{ip,t}^{Grid\to GB} + g_{ip,t}^{Grid\to GS} - g_{ip,t}^{GS\to Grid}}_{g_{ip,t}^{Exch}}\right) \tag{6c}$$

Equations (6d)-(6i) model the flow of power, gas, and heat input to industrial park components. (6d) and (6e) model the gas flow entering the CHP unit and the GB, respectively. (6f) models the input power flow to the electric heater, while (6g)-(6i) model the flow of electricity, heat, and gas input to the ES, TS, and GS systems, respectively.

$$g_{ip,t}^{CHP} = g_{ip,t}^{Grid\to CHP} + g_{ip,t}^{GS\to CHP} \tag{6d}$$

$$g_{ip,t}^{GB} = g_{ip,t}^{Grid\to GB} + g_{ip,t}^{GS\to GB} \tag{6e}$$

$$p_{ip,t}^{EH} = p_{ip,t}^{Grid\to EH} + p_{ip,t}^{ES\to EH} + p_{ip,t}^{RES\to EH} \tag{6f}$$

$$p_{ip,t}^{ES,Ch} = p_{ip,t}^{Grid\to ES} + p_{ip,t}^{RES\to ES} + p_{ip,t}^{CHP\to ES} \tag{6g}$$

$$h_{ip,t}^{TS,Ch} = h_{ip,t}^{CHP\to TS} + h_{ip,t}^{GB\to TS} + h_{ip,t}^{EH\to TS} \tag{6h}$$

$$g_{ip,t}^{GS,Ch} = g_{ip,t}^{Grid\to GS} \tag{6i}$$

The flow of active and reactive power, gas, and heat output from the components is presented in (6j)-(6t). Equations (6j)-(6l) detail the flow of active, reactive, and heating power output from the CHP unit. Equations (6m) and (6n) describe the heat flow from the GB and electric heater, respectively. Equations (6o) and (6p) represent the flow of active and reactive power output from the renewable units, respectively. Equation (6q) details the reactive power flow of the capacitor bank. Finally, (6r)-(6t) model the flow of power, heat, and gas output from the ES, TS, and GS systems, respectively.

$$p_{ip,t}^{CHP} = p_{ip,t}^{CHP\to Grid} + p_{ip,t}^{CHP\to ES} + p_{ip,t}^{CHP\to EH} + p_{ip,t}^{CHP\to Load} \tag{6j}$$

$$q_{ip,t}^{CHP} = q_{ip,t}^{CHP\to Grid} + q_{ip,t}^{CHP\to Load} \tag{6k}$$

$$h_{ip,t}^{CHP} = h_{ip,t}^{CHP\to TS} + h_{ip,t}^{CHP\to Load} \tag{6l}$$

$$h_{ip,t}^{GB} = h_{ip,t}^{GB\to TS} + h_{ip,t}^{GB\to Load} \tag{6m}$$

$$h_{ip,t}^{EH} = h_{ip,t}^{EH\to TS} + h_{ip,t}^{EH\to Load} \tag{6n}$$

$$P_{ip,t}^{WU} + P_{ip,t}^{SU} = p_{ip,t}^{RES\to Grid} + p_{ip,t}^{RES\to ES} + p_{ip,t}^{RES\to EH} + p_{ip,t}^{RES\to Load} \quad (6o)$$

$$q_{ip,t}^{WU} + q_{ip,t}^{SU} = q_{ip,t}^{RES\to Grid} + q_{ip,t}^{RES\to Load} \quad (6p)$$

$$q_{ip,t}^{CB} = q_{ip,t}^{CB\to Grid} + q_{ip,t}^{CB\to Load} \quad (6q)$$

$$p_{ip,t}^{ES,Dis} = p_{ip,t}^{ES\to Grid} + p_{ip,t}^{ES\to EH} + p_{ip,t}^{ES\to Load} \quad (6r)$$

$$h_{ip,t}^{TS,Dis} = h_{ip,t}^{TS\to Load} \quad (6s)$$

$$g_{ip,t}^{GS,Dis} = g_{ip,t}^{GS\to Grid} + g_{ip,t}^{GS\to CHP} + g_{ip,t}^{GS\to GB} + g_{ip,t}^{GS\to Load} \quad (6t)$$

- **Industrial Park Tasks**

Equations (7a)-(7f) describe the tasks required to produce materials 1 to 6 [50]. W is a parameter that converts consumed loads into materials. (7g) models the upper and lower limits of the production of each material at any given time. (7h) states that changes in the production volume of the final product ($\Delta m5_{ip,t}^{Product}$) are determined based on the differences between values planned for the normal operating condition ($M5_{ip,t}^{Product,DA}$) and the values obtained during the current emergency period planning ($m5_{ip,t}^{Product}$). (7i) confines the changes in the production volume. (7j)-(7o) model the warehouses related to materials 1 to 6, respectively. These equations state that the volume of materials in each warehouse at time t depends on the volume of materials remaining from the previous time and the import and export of materials in the current time. (7p) models the upper and lower hourly limits for the volume of materials stored in the warehouse, while (7q) specifies the initial volume of materials in each warehouse at the start of the planning period.

$$m1_{ip,t}^{T1} = W^{P,T1} p_{ip,t}^{T1} \quad (7a)$$

$$m2_{ip,t}^{T2} = W^{P,T2} p_{ip,t}^{T2} + W^{G,T2} g_{ip,t}^{T2} + W^{M1,T2} m1_{ip,t}^{T2} + W^{M6,T2} m6_{ip,t}^{T2} \quad (7b)$$

$$m3_{ip,t}^{T3} = W^{P,T3} p_{ip,t}^{T3} + W^{G,T3} g_{ip,t}^{T3} + W^{M6,T3} m6_{ip,t}^{T3} \quad (7c)$$

$$m4_{ip,t}^{T4} = W^{P,T4} p_{ip,t}^{T4} \quad (7d)$$

$$m5_{ip,t}^{T5} = W^{P,T5} p_{ip,t}^{T5} + W^{H,T5} h_{ip,t}^{T5} + W^{M2,T5} m2_{ip,t}^{T5} + W^{M3,T5} m3_{ip,t}^{T5} + W^{M4,T5} m4_{ip,t}^{T5} + W^{M6,T5} m6_{ip,t}^{T5} \quad (7e)$$

$$m6_{ip,t}^{T6} = W^{P,T6} p_{ip,t}^{T6} \quad (7f)$$

$$(m)_{ip,t}^{T1-T6,\min} \le (m)_{ip,t}^{T1-T6} \le (m)_{ip,t}^{T1-T6,\max} \quad (7g)$$

$$\Delta m5_{ip,t}^{Product} = M5_{ip,t}^{Product,Normal} - m5_{ip,t}^{Product} \quad (7h)$$

$$\Delta M5_{ip,t}^{Product,\min} \le \Delta m5_{ip,t}^{Product} \le \Delta M5_{ip,t}^{Product,max} \quad (7i)$$

$$e_{ip,t}^{S1} = e_{ip,t-1}^{S1} + \left(m1_{ip,t}^{T1}\right) - \left(m1_{ip,t}^{T2}\right) \quad (7j)$$

$$e_{ip,t}^{S2} = e_{ip,t-1}^{S2} + \left(m2_{ip,t}^{T2}\right) - \left(m2_{ip,t}^{T5}\right) \quad (7k)$$

$$e_{ip,t}^{S3} = e_{ip,t-1}^{S3} + \left(m3_{ip,t}^{T3}\right) - \left(m3_{ip,t}^{T5}\right) \quad (7l)$$

$$e_{ip,t}^{S4} = e_{ip,t-1}^{S4} + \left(m4_{ip,t}^{T4}\right) - \left(m4_{ip,t}^{T5}\right) \quad (7m)$$

$$e_{ip,t}^{S5} = e_{ip,t-1}^{S5} + \left(m5_{ip,t}^{T5}\right) - \left(m5_{ip,t}^{Product}\right) \quad (7n)$$

$$e_{ip,t}^{S6} = e_{ip,t-1}^{S6} + \left(m6_{ip,t}^{T6}\right) - \left(m6_{ip,t}^{T2} + m6_{ip,t}^{T3} + m6_{ip,t}^{T5}\right) \quad (7o)$$

$$E_{ip}^{S1-S6,\min} \le e_{ip,t}^{S1-S6} \le E_{ip}^{S1-S6,\max} \quad (7p)$$

$$e_{ip,t=0}^{S1-S6} = E_{ip}^{S1-S6,Initial} \quad (7q)$$

Equations (7q)-(7t) respectively provide the active, reactive, gas, and thermal load suppliers required to perform tasks. These loads can be supplied through internal components of the industrial park or from electricity and gas networks. Equation (7u) relates the reactive power required by each task to its active power consumption using the χ parameter.

$$p_{ip,t}^{CHP\to Load} + p_{ip,t}^{ES\to Load} + p_{ip,t}^{RES\to Load} + p_{ip,t}^{Grid\to Load} = p_{ip,t}^{T1} + p_{ip,t}^{T2} + p_{ip,t}^{T3} + p_{ip,t}^{T4} + p_{ip,t}^{T5} + p_{ip,t}^{T6} \quad (7q)$$

$$q_{ip,t}^{Grid\to Load} + q_{ip,t}^{CB\to Load} + q_{ip,t}^{RES\to Load} = q_{ip,t}^{T1} + q_{ip,t}^{T2} + q_{ip,t}^{T3} + q_{ip,t}^{T4} + q_{ip,t}^{T5} + q_{ip,t}^{T6} \quad (7r)$$

$$g_{ip,t}^{GS\to Load} + g_{ip,t}^{Grid\to Load} = g_{ip,t}^{T2} + g_{ip,t}^{T3} \quad (7s)$$

$$h_{ip,t}^{CHP\to Load} + h_{ip,t}^{GB\to Load} + h_{ip,t}^{HS\to Load} + h_{ip,t}^{EH\to Load} = h_{ip,t}^{T5} \quad (7t)$$

$$q_{ip,t}^{T1-T6} = \chi^{T1-T6} p_{ip,t}^{T1-T6} \quad (7u)$$

3.2.2. P2H units

The P2H units under investigation incorporate local wind and solar systems, an electrolyzer, and a HS. Under normal operating conditions, these P2H units sell their produced hydrogen to customers under contract. During emergency operating conditions, they can sell part of their hydrogen to the system operator, which is then converted into electricity via fuel cell-equipped trucks and subsequently injected into the network.

The objective function of the P2H unit, presented in (3), is modeled to maximize the sales of emergency services ($h2_{hu,t}^{Service}\lambda_{hu,t}^{H2,Service}$) while minimizing the costs associated with changes in predetermined exchanges with customers ($\Delta h2_{hs,t}^{Customers}\pi_{hu,t}^{Customers}$). Equation (8a) calculates changes in P2H unit exchanges based on the difference between the normal operating condition ($H2_{hs,t}^{Customers,Normal}$) and the finalized exchanges during the emergency planning period ($h2_{hs,t}^{Customers}$). (8b) limits the range of changes in transactions with customers. In (8c), the electrolyzer is modeled. This equipment converts the power received from wind and solar systems ($P_{hu,t}^{WU} + P_{hu,t}^{SU}$) into hydrogen, taking into account the efficiency factor η^{EL} and the lower heating value (LHV^{H2}). It should be noted that the HS system within the P2H unit adheres to the formulation provided for these systems in the routing subsection. (8d) states that all the hydrogen produced by the electrolyzer ($h2_{hu,t}^{EL}$) is directly stored in the HS system ($h2_{hu,t}^{Ch}$). Finally, (8e) specifies that the hydrogen discharged from the HS system ($h2_{hs,t}^{Dis}$) is either sold to customers or provided to the system operator as emergency services.

$$\max of_{hu} = \sum_t \left(h2_{hu,t}^{Service}\lambda_{hu,t}^{H2,Service}\right) - \left(\Delta h2_{hu,t}^{Customers}\pi^{H2,Price}\right) \quad (3)$$

$$\Delta h2_{hu,t}^{Customers} = H2_{hu,t}^{Customers,Normal} - h2_{hu,t}^{Customers} \quad (8a)$$

$$\Delta H2_{hu,t}^{Customers,min} \le \Delta h2_{hu,t}^{Customers} \le \Delta H2_{hu,t}^{Customers,max} \quad (8b)$$

$$h2_{hu,t}^{EL} = \frac{\eta^{EL}\left(P_{hu,t}^{WU} + P_{hu,t}^{SU}\right)}{LHV^{H2}} \quad (8c)$$

$$h2_{hu,t}^{EL} = h2_{hu,t}^{Ch} \quad (8d)$$

Table 2
Pseudocode of proposed self-healing mechanism using augmented ADMM algorithm.

Inputs: Power and gas networks data, Smart prosumers data, Information of fuel cell-equipped trucks.
Initialization:
Placed fuel cell-equipped trucks at starting point.
Planned repairing process for damaged lines and pipelines.
For iteration $r = 1$ to r^{Max}, **Do**:
Solve first stage optimization model (Eq. (1))
Generate emergency pulses for smart prosumers at connection points.
For industrial park $ip = 1$ to ip^{Max}, **Do**:
Solve second stage optimization problem for ip based on power and gas emergency pulses (Eq. (2)).
Fix optimal participation in emergency services for ip.
End
For P2H unit $pu = 1$ to pu^{Max}, **Do**:
Solve second stage optimization problem for pu based on hydrogen emergency pulses (Eq. (3)).
Fix optimal participation in emergency services for pu.
End
For charging station $cs = 1$ to cs^{Max}, **Do**:
Solve second stage optimization problem for cs based on power emergency pulses (Eq. (4)).
Fix optimal participation in emergency services for cs.
End
If iteration number is grater than 1, **Then**:
Update emergency services prices by:

$$\lambda^{P,Service,r+1}_{ip/cs,t} = \lambda^{P,Service,r}_{ip/cs,t} + \rho^{P,r}_{ip/cs}\left(p^{Exch}_{ip/cs,t} - \hat{p}^{Exch}_{ip/cs,t}\right)$$

$$\lambda^{Q,Service,r+1}_{ip/cs,t} = \lambda^{Q,Service,r}_{ip/cs,t} + \rho^{Q,r}_{ip/cs}\left(q^{Exch}_{ip/cs,t} - \hat{q}^{Exch}_{ip/cs,t}\right)$$

$$\lambda^{G,Service,r+1}_{ip,t} = \lambda^{P,Service,r}_{ip,t} + \rho^{G,r}_{ip}\left(g^{Exch}_{ip,t} - \hat{g}^{Exch}_{ip,t}\right)$$

$$\lambda^{H2,Service,r+1}_{hu,t} = \lambda^{H2,Service,r}_{hu,t} + \rho^{H2,r}_{hu}\left(h2^{Exch}_{hu,t} - \hat{h2}^{Exch}_{hu,t}\right)$$

End
If primal residual if grater than dual residual, **Then**:

$$\rho^{P/Q/G/H2,r+1}_{ip/hu/cs} = \rho^{P/Q/G/H2,r}_{ip/hu/cs}\left(1 + \log\left(\frac{R^{P/Q/G/H2,Primal}_{ip/hu/cs}}{R^{P/Q/G/H2,Dual}_{ip/hu/cs}}\right)\right)$$

ElseIf dual residual if grater than primal residual, **Then**:

$$\rho^{P/Q/G/H2,r+1}_{ip/hu/cs} = \rho^{P/Q/G/H2,r}_{ip/hu/cs}\left(1 + \log\left(\frac{R^{P/Q/G/H2,Primal}_{ip/hu/cs}}{R^{P/Q/G/H2,Dual}_{ip/hu/cs}}\right)\right)^{-1}$$

Else:

$$\rho^{P/Q/G/H2,r+1}_{ip/hu/cs} = \rho^{P/Q/G/H2,r}_{ip/hu/cs}$$

End
End

$$h2^{Dis}_{hu,t} = h2^{Customers}_{hu,t} + h2^{Service}_{hu,t} \tag{8e}$$

3.2.3. Charging stations

The charging stations under study are equipped with solar panels and fast charging systems for EVs and are capable of providing V2G services [51]. (4) presents the objective function of the charging stations, which is modeled as the maximization of their emergency services minus the costs associated with changes in their normal schedule ($\Delta p^{Charger}_{cs,t}\pi^{P,Price}_{t}$). Equations (9a)-(9f) model the limitations of EV batteries. Specifically, in (9a), the battery energy level of cars is determined every hour. (9b) and (9c) model the hourly charging and discharging limits, while (9d) models the upper and lower limits of the battery charge level. (9e) determines the range of the battery charge level when leaving the station, and finally, (9f) limits the charging and discharging of cars to their presence in the station.

Equations (9g)-(9l) model the constraints related to the charging station operator. (9g) states that the load of the charging station at time t ($p^{Charger}_{cs,t}$) is determined by the charge/discharge status of the batteries of the connected cars. (9h) models the limitation of active and reactive powers of the charging station. Active ($p^{Service}_{cs,t}$) and reactive ($q^{Service}_{cs,t}$) power emergency services that can be provided to the system operator are calculated by (9i) and (9j), respectively. These services are calculated based on the difference between the station's load during normal ($P^{Exch,Normal}_{cs,t}$/ $Q^{Exch,Normal}_{cs,t}$) and emergency operating conditions. Equation (9k) calculates the changes in the cars' charging schedules ($\Delta p^{Charger}_{cs,t}$) considering both normal and emergency states. Lastly, constraint (9l) limits these changes.

$$\max of_{cs} = \sum_{t}\left(p^{Service}_{cs,t}\lambda^{P,Service}_{cs,t} + q^{Service}_{cs,t}\lambda^{Q,Service}_{cs,t}\right) - \sum_{t}\left(\Delta p^{Charger}_{cs,t}\pi^{P,Price}_{t}\right) \tag{4}$$

$$e^{EV}_{ev,t} = e^{EV}_{ev,t-1} + \left(p^{Ch}_{ev,t}\eta^{Ch} - \frac{p^{Dis}_{ev,t}}{\eta^{Dis}}\right)\Delta t \tag{9a}$$

$$0 \le p^{Ch}_{ev,t} \le P^{Ch,\max}_{ev,t} i^{Ch}_{ev,t} \tag{9b}$$

$$0 \le p^{Dis}_{ev,t} \le P^{Dis,\max}_{ev,t} i^{Dis}_{ev,t} \tag{9c}$$

$$E^{EV,\min}_{ev} \le e^{EV}_{ev,t} \le E^{EV,\max}_{ev} \tag{9d}$$

$$E^{Departure,\min}_{ev} \le e_{ev,t=Departure} \le E^{Departure,\max}_{ev} \tag{9e}$$

$$i^{Ch}_{ev,t} + i^{Dis}_{ev,t} \le I^{Parking}_{ev,t} \tag{9f}$$

$$p^{Charger}_{cs,t} = \sum_{ev\in\Upsilon^{ev}_{cs}}\left(p^{Ch}_{ev,t} - p^{Dis}_{ev,t}\right) \tag{9g}$$

$$\left(p^{Charger}_{cs,t}\right)^2 + \left(q^{Charger}_{cs,t}\right)^2 \le \left(S^{Charger}_{cs,t}\right)^2 \tag{9h}$$

$$p^{Service}_{cs,t} = P^{Exch,Normal}_{cs,t} - \left(\underbrace{q^{Charger}_{cs,t} - P^{SU}_{cs,t} + p^{Ch}_{cs,t} - p^{Dis}_{cs,t}}_{p^{Exch}_{cs,t}}\right) \tag{9i}$$

$$q^{Service}_{cs,t} = Q^{Exch,Normal}_{cs,t} - \left(\underbrace{q^{Charger}_{cs,t} + q^{SU}_{cs,t}}_{q^{Exch}_{cs,t}}\right) \tag{9j}$$

$$\Delta p^{Charger}_{cs,t} = P^{Charger,Normal}_{cs,t} - p^{Charger}_{cs,t} \tag{9k}$$

$$\Delta P^{Charger,\min}_{cs,t} \le \Delta p^{Charger}_{cs,t} \le \Delta P^{Charger,\max}_{cs,t} \tag{9l}$$

3.3. The proposed augmented ADMM for secure management of interactions

The Augmented ADMM introduced in our work represents a critical advancement over the traditional ADMM algorithm, particularly in the context of decentralized optimization for self-healing in coordinated electricity and gas networks. The proposed augmented variant is designed to enhance convergence speed, improve resilience during emergency conditions, and ensure secure management of interactions between the system operator and smart prosumers, including industrial parks, P2H units, and charging stations.

Equations (10a)-(10d) represent the penalty terms associated with the exchange of active power, reactive power, gas, and hydrogen between the entities, respectively [52]. $\rho^{P,r}_{ip/cs}$ represents the penalty factor of the ADMM. The parameters with hats represent the values of the services from the operator's point of view, while the parameters without hats represent the values of the services from the perspective of the prosumers. Equations (10e)-(10h) describe the updates of the Lagrange multipliers (λ) for the services provided. The multipliers $\lambda^{P,Service,r+1}_{ip/cs,t}$, $\lambda^{Q,Service,r+1}_{ip/cs,t}$, $\lambda^{G,Service,r+1}_{ip,t}$, and $\lambda^{H2,Service,r+1}_{hu,t}$ are iteratively adjusted based on differences between the services requested by the operator and the

services provided by the prosumers. Equations (10i)-(10l) define the primal residuals for active power ($R_{ip/cs}^{P,Primal}$), reactive power ($R_{ip/cs}^{Q,Primal}$), gas ($R_{ip}^{G,Primal}$), and hydrogen ($R_{hu}^{H2,Primal}$). These residuals measure the differences in values obtained for the coupling variables from the perspectives of two opposing entities. Equations (10m)-(10p) define the dual residuals for active power ($R_{ip/cs}^{P,Dual}$), reactive power ($R_{ip/cs}^{Q,Dual}$), gas ($R_{ip}^{G,Dual}$), and hydrogen ($R_{hu}^{H2,Dual}$). These residuals measure the change in the Lagrange multipliers between iterations.

The original ADMM algorithm operates on a dual decomposition method that facilitates distributed optimization by decoupling the original problem into subproblems. However, it suffers from slow convergence rates in large-scale, high-dimensional optimization settings, primarily due to the fixed penalty parameters that are static throughout iterations. To address this limitation, the Augmented ADMM integrates a dynamic penalty update mechanism governed by logarithmic terms, which adaptively adjusts the penalty coefficients in each iteration based on the relative magnitudes of the primal and dual residuals. In this context, (10q)-(10t) describe the augmented update rules for the penalty parameters ($\rho_{ip/cs}^{P,r}$). These rules adjust the penalty parameters based on the ratio of primal to dual residuals, ensuring that the algorithm maintains a balance between primal and dual feasibility. The parameters μ is used to determine the adjustment factor, promoting convergence by scaling the penalties appropriately. Finally, (10u) calculates the overall convergence criterion (δ), which aggregates the primal and dual residuals across all services. This criterion provides a comprehensive measure of the system's convergence, indicating whether the ADMM algorithm has achieved an optimal and stable solution for coordinating the exchange of power, gas, and hydrogen services during emergency situations. Table 2 provides a pseudocode to facilitate the simulation of the distributed coordination mechanism using the proposed augmented ADMM. By systematically updating the exchange values and Lagrange multipliers while adapting the penalty parameters, this augmented ADMM framework ensures robust and efficient coordination between the system operator and smart prosumers, enhancing the resilience and stability of the energy network during emergencies.

$$\frac{\rho_{ip/cs}^{P,r}}{2}\left\|\widehat{p}_{ip/cs,t}^{Exch}-p_{ip/cs,t}^{Exch}\right\|_2^2 \tag{10a}$$

$$\frac{\rho_{ip/cs}^{Q,r}}{2}\left\|\widehat{q}_{ip/cs,t}^{Exch}-q_{ip/cs,t}^{Exch}\right\|_2^2 \tag{10b}$$

$$\frac{\rho_{ip}^{G,r}}{2}\left\|\widehat{g}_{ip,t}^{Exch}-g_{ip,t}^{Exch}\right\|_2^2 \tag{10c}$$

$$\frac{\rho_{hu}^{H2,r}}{2}\left\|\widehat{h2}_{hu,t}^{Exch}-h2_{hu,t}^{Exch}\right\|_2^2 \tag{10d}$$

$$\lambda_{ip/cs,t}^{P,Service,r+1}=\lambda_{ip/cs,t}^{P,Service,r}+\rho_{ip/cs}^{P,r}\left(p_{ip/cs,t}^{Exch}-\widehat{p}_{ip/cs,t}^{Exch}\right) \tag{10e}$$

$$\lambda_{ip/cs,t}^{Q,Service,r+1}=\lambda_{ip/cs,t}^{Q,Service,r}+\rho_{ip/cs}^{Q,r}\left(q_{ip/cs,t}^{Exch}-\widehat{q}_{ip/cs,t}^{Exch}\right) \tag{10f}$$

$$\lambda_{ip,t}^{G,Service,r+1}=\lambda_{ip,t}^{P,Service,r}+\rho_{ip}^{G,r}\left(g_{ip,t}^{Exch}-\widehat{g}_{ip,t}^{Exch}\right) \tag{10g}$$

$$\lambda_{hu,t}^{G,Service,r+1}=\lambda_{hu,t}^{H2,Service,r}+\rho_{hu}^{H2,r}\left(h2_{hu,t}^{Exch}-h2_{hu,t}^{Exch}\right) \tag{10h}$$

$$R_{ip/cs}^{P,Primal}=\left\|\widehat{p}_{ip/cs,t}^{Exch}-p_{ip/cs,t}^{Exch}\right\|_2 \tag{10i}$$

$$R_{ip/cs}^{Q,Primal}=\left\|\widehat{q}_{ip/cs,t}^{Exch}-q_{ip/cs,t}^{Exch}\right\|_2 \tag{10j}$$

$$R_{ip}^{G,Primal}=\left\|\widehat{g}_{ip,t}^{Exch}-g_{ip,t}^{Exch}\right\|_2 \tag{10k}$$

$$R_{hu}^{H2,Primal}=\left\|\widehat{h2}_{hu,t}^{Exch}-h2_{hu,t}^{Exch}\right\|_2 \tag{10l}$$

$$R_{ip/cs}^{P,Dual}=\left\|\lambda_{ip/cs,t}^{P,Service,r+1}-\lambda_{ip/cs,t}^{P,Service,r}\right\|_2 \tag{10m}$$

$$R_{ip/cs}^{Q,Dual}=\left\|\lambda_{ip/cs,t}^{Q,Service,r+1}-\lambda_{ip/cs,t}^{Q,Service,r}\right\|_2 \tag{10n}$$

$$R_{ip}^{G,Dual}=\left\|\lambda_{ip,t}^{G,Service,r+1}-\lambda_{ip,t}^{G,Service,r}\right\|_2 \tag{10o}$$

$$R_{hu}^{H2,Dual}=\left\|\lambda_{hu,t}^{H2,Service,r+1}-\lambda_{hu,t}^{H2,Service,r}\right\|_2 \tag{10p}$$

$$\rho_{ip/cs}^{P,r+1}=\begin{cases}\rho_{ip/cs}^{P,r}\left(1+\log\left(\dfrac{R_{ip/cs}^{P,Primal}}{R_{ip/cs}^{P,Dual}}\right)\right) & \text{if} \quad R_{ip/cs}^{P,Primal}\geq\mu R_{ip/cs}^{P,Dual}\\ \rho_{ip/cs}^{P,r}\left(1+\log\left(\dfrac{R_{ip/cs}^{P,Primal}}{R_{ip/cs}^{P,Dual}}\right)\right)^{-1} & \text{if} \quad R_{ip/cs}^{P,Dual}\geq\mu R_{ip/cs}^{P,Primal}\\ \rho_{ip/cs}^{P,r}, Otherwise\end{cases} \tag{10q}$$

$$\rho_{ip}^{G,r+1}=\begin{cases}\rho_{ip}^{G,r}\left(1+\log\left(\dfrac{R_{ip}^{G,Primal}}{R_{ip}^{G,Dual}}\right)\right) & \text{if} \quad R_{ip}^{G,Primal}\geq\mu R_{ip}^{G,Dual}\\ \rho_{ip}^{G,r}\left(1+\log\left(\dfrac{R_{ip}^{G,Primal}}{R_{ip}^{G,Dual}}\right)\right)^{-1} & \text{if} \quad R_{ip}^{G,Dual}\geq\mu R_{ip}^{G,Primal}\\ \rho_{ip}^{G,r}, Otherwise\end{cases} \tag{10r}$$

$$\rho_{ip/cs}^{Q,r+1}=\begin{cases}\rho_{ip/cs}^{Q,r}\left(1+\log\left(\dfrac{R_{ip/cs}^{Q,Primal}}{R_{ip/cs}^{Q,Dual}}\right)\right) & \text{if} \quad R_{ip/cs}^{Q,Primal}\geq\mu R_{ip/cs}^{Q,Dual}\\ \rho_{ip/cs}^{Q,r}\left(1+\log\left(\dfrac{R_{ip/cs}^{Q,Primal}}{R_{ip/cs}^{Q,Dual}}\right)\right)^{-1} & \text{if} \quad R_{ip/cs}^{Q,Dual}\geq\mu R_{ip/cs}^{Q,Primal}\\ \rho_{ip/cs}^{Q,r}, Otherwise\end{cases} \tag{10s}$$

$$\rho_{hu}^{H2,r+1}=\begin{cases}\rho_{hu}^{H2,r}\left(1+\log\left(\dfrac{R_{hu}^{H2,Primal}}{R_{hu}^{H2,Dual}}\right)\right) & \text{if} \quad R_{hu}^{H2,Primal}\geq\mu R_{hu}^{H2,Dual}\\ \rho_{hu}^{H2,r}\left(1+\log\left(\dfrac{R_{hu}^{H2,Primal}}{R_{hu}^{H2,Dual}}\right)\right)^{-1} & \text{if} \quad R_{hu}^{H2,Dual}\geq\mu R_{hu}^{H2,Primal}\\ \rho_{hu}^{H2,r}, Otherwise\end{cases} \tag{10t}$$

$$\delta=\left\|R_{ip/cs}^{P,Primal}+R_{ip/cs}^{P,Dual}+R_{ip/cs}^{Q,Primal}+R_{ip/cs}^{Q,Dual}+R_{ip}^{G,Primal}+R_{ip}^{G,Dual}+R_{hu}^{H2,Primal}+R_{hu}^{H2,Dual}\right\|_2 \tag{10u}$$

Table 3
Specifications of scenarios studied.

Scenario	Automatic Switching	P2H Units	Industrial Parks	Charging Stations	Fault Location	Coordinator	Studied System	
1	×	×	×	×	Electricity Network	Augmented ADMM	Electricity	Gas
2	✓	×	×	×	Electricity Network	Augmented ADMM	118-Bus	65-Node
3	✓	✓	×	×	Electricity Network	Augmented ADMM	118-Bus	65-Node
4	✓	✓	✓	×	Electricity Network	Augmented ADMM	118-Bus	65-Node
5	✓	✓	✓	✓	Electricity Network	Augmented ADMM	118-Bus	65-Node
6	✓	×	×	×	Gas Network	Augmented ADMM	118-Bus	65-Node
7	✓	×	✓	×	Gas Network	Augmented ADMM	118-Bus	65-Node
8	✓	×	✓	×	Gas Network	Original ADMM	118-Bus	65-Node
9	✓	✓	✓	✓	Electricity Network	Augmented ADMM	136-Bus	130-Node

4. Methodological framework

This section presents a systematic breakdown of the proposed self-healing mechanism for coordinated electricity and gas networks, outlining the steps for model initialization, data preprocessing, decentralized optimization, and emergency service coordination, distinct from the formal mathematical formulations previously discussed.

4.1. - data preprocessing and initialization

The initial step involves data collection and preprocessing, where network parameters, emergency service capabilities, and prosumer characteristics are configured. This includes:

- Loading network topology for both electricity and gas infrastructures.
- Defining the operational characteristics of industrial parks, P2H units, and charging stations.
- Specifying the mobility and energy capacities of fuel cell-equipped trucks.

These parameters are input into the optimization model, ensuring consistency across both infrastructures for coordinated self-healing operations.

4.2. Model initialization

The augmented ADMM mechanism is initialized with:

- Penalty parameters for primal and dual updates.
- Initial values for distributed decision variables.
- Communication links established between the system operator and smart prosumers.

The decentralized nature of the model allows each agent to operate with local information, reducing the need for central data aggregation.

4.3. Coordination strategy and decentralized optimization

The space-time network model is engaged to optimize the dispatch of mobile energy resources during emergency scenarios. The steps include:

- Local optimization at each prosumer node using the augmented ADMM update rules.
- Real-time adjustments of penalty parameters based on primal and dual residuals.
- Iterative coordination between the system operator and prosumers for convergence.

This decentralized strategy ensures rapid stabilization without extensive central intervention, enhancing resilience and privacy.

4.4. Emergency service dispatch and self-healing

The final step focuses on the execution of self-healing operations:

- **Fuel cell-equipped trucks** are optimally routed to critical points in the network based on real-time assessments.
- **Industrial parks** and **P2H units** dynamically adjust their load consumption and emergency service provision.
- Load shedding is minimized through efficient redistribution of resources, ensuring secure and stable operation during crisis events.

The proposed methodological steps are designed to optimize system recovery and maintain operational stability during critical disruptions, demonstrating the effectiveness of the augmented ADMM algorithm in real-world decentralized network scenarios.

5. Results and discussion

In this section, the proposed two-stage self-healing mechanism is applied to two distinct test systems. The first system comprises a modified 118-bus electrical distribution network [53] paired with a 65-node gas distribution network [54], while the second system includes a modified 123-bus electrical distribution network [55] alongside a modified 130-node gas distribution network [54]. It is tested across nine scenarios described in Table 3, designed to assess the impact of automatic switching, prosumer participation, and the augmented ADMM algorithm on the system's technical, economic, and resilience indicators. In scenarios 1 to 5, it is assumed that an error occurs in the electrical network, leading to the outage of lines 27 (between buses 4 and 28) and 88 (between buses 64 and 89) for 7 h (from 10 a.m. to 4 p.m.). In cases 6 to 8, it is assumed that the electrical network is healthy, but the volume of injected gas from station decreases by 25 % for 5 h (from 2:00 p.m. to 6:00 p.m.). Fig. 4 presents an overview of the first test system, illustrating its integration with six industrial parks, nine P2H units, and twelve charging stations. This network has 20 lines equipped with automatic switches, marked in red. Nodes with critical loads are highlighted with Green. The generation units connected to the electric grid include four dispatchable units, three wind units, and fourteen solar units, with each renewable unit integrated with an ES system. This network has three compressors and four GS systems, receiving gas through an injection station connected to node 1. Table 4 outlines the specifications of smart prosumers, while Fig. 5a and b illustrate the power and gas purchase prices from upstream grids. Fig. 6a–h present the input parameters for the system operator and smart prosumers.

5.1. Scenarios 1 & 2

This subsection presents the simulation results for scenarios 1 and 2, where self-healing planning is performed without smart prosumer participation. In scenario 1, the electrical network topology is fixed, whereas in scenario 2, the operator can adjust it dynamically. The results in Tables 5 and 6 show that the activation of automatic switching in scenario 2 reduces load shedding by 34.39 % and operating costs by

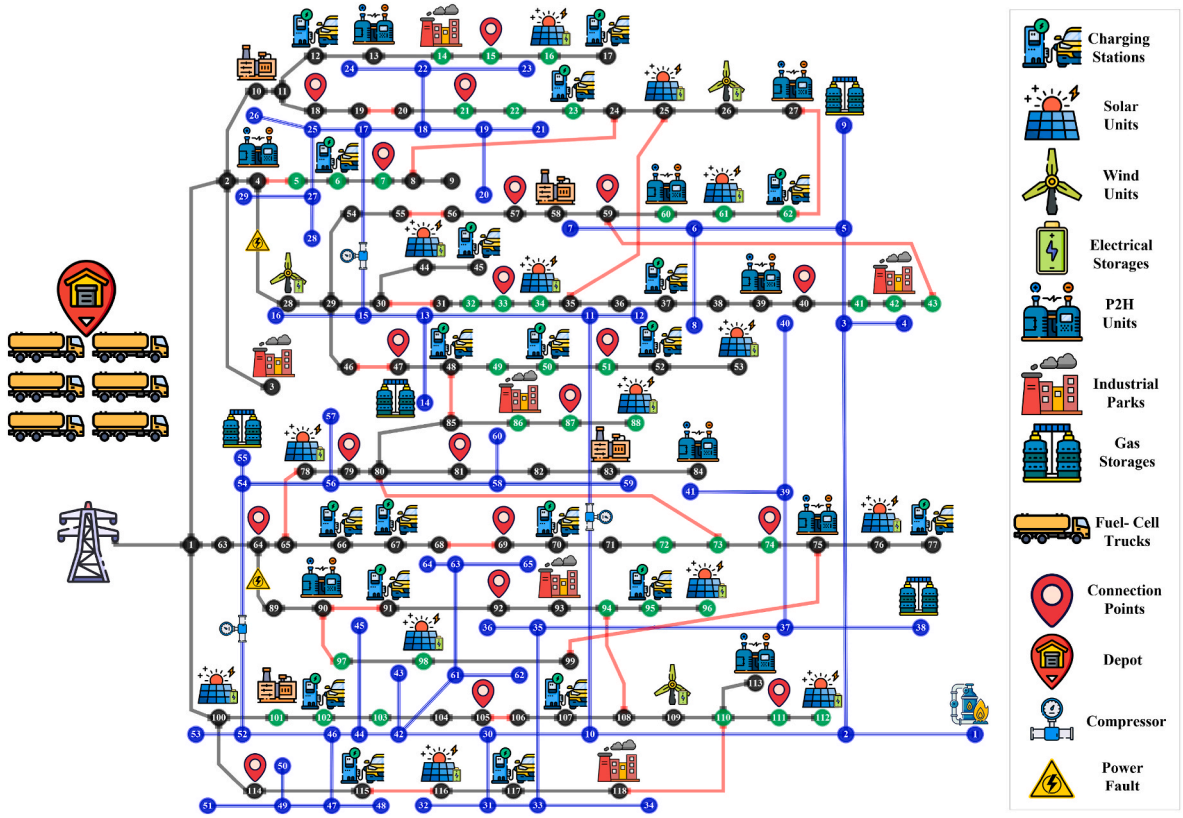

Fig. 4. Overview of the first test system [53,54].

Table 4
Information on smart prosumers.

Industrial Parks					
Unit Number		Connection Points			Production Capacity (item)
		Power	Gas		
1		14	22		127
2		42	4		159
3		3	16		117
4		86	60		180
5		93	65		106
6		118	34		138
P2H Units			Charging Stations		
Unit Numbers	Connection Points	Peak Demand (kg)	Unit Numbers	Connection Points	Peak Demand (kW)
1-2-3	13-39-113	250	1–7	12-6-37-66-107-77-62	600
4-5-6	4-90-84	300	8–14	17-23-67-102-115-50-45	800
7-8-9	27-60-75	200	15–20	48-52-70-91-95-117	700

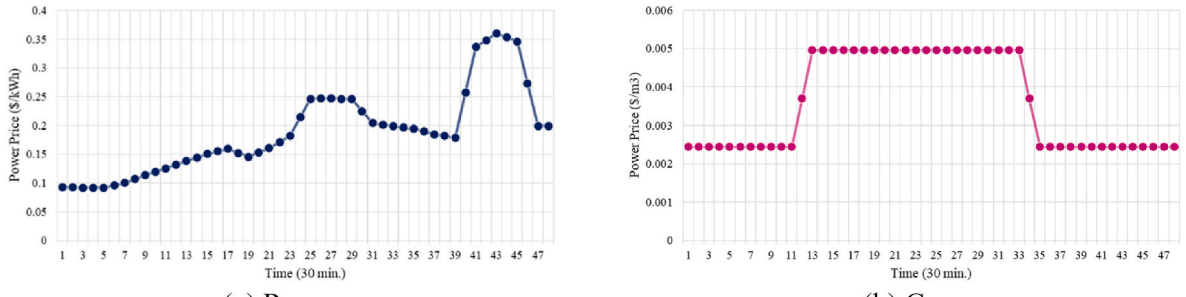

Fig. 5. Purchasing prices of power and gas from upstream grids.

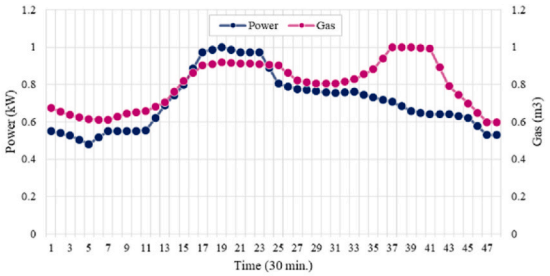

(a) System operator's planned upstream grid exchanges under normal conditions

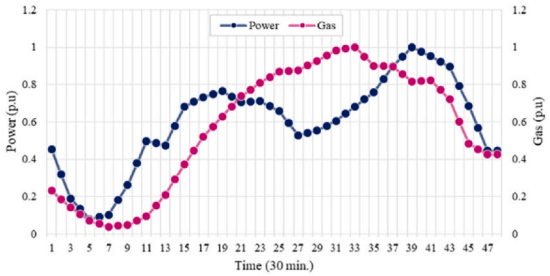

(b) System operator's demand under normal conditions

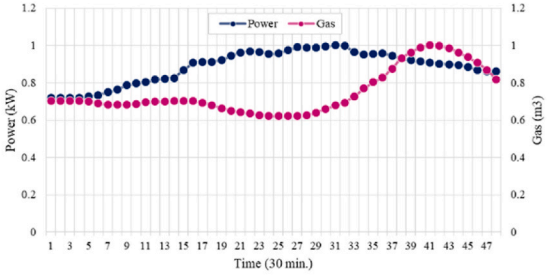

(c) Industrial parks' planned grid exchanges under normal conditions

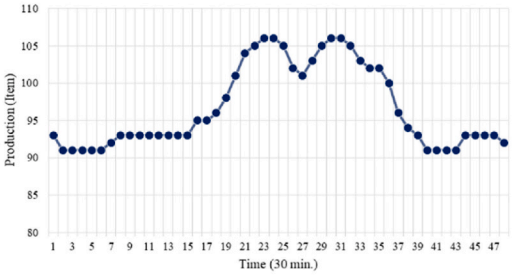

(d) Industrial parks' production under normal conditions

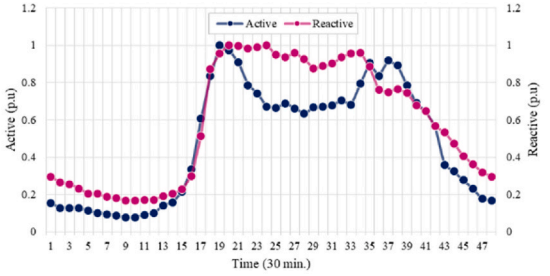

(e) Charging stations' planned grid exchanges under normal conditions

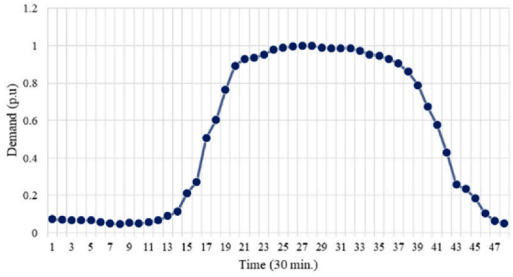

(f) Charging stations' demand under normal conditions

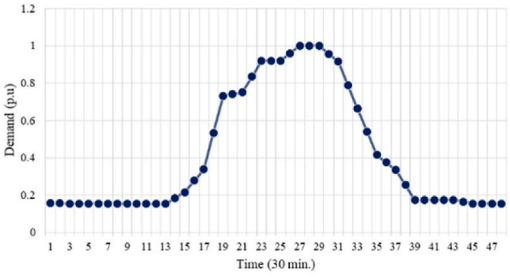

(g) P2H units' hydrogen sold to their customers under normal conditions

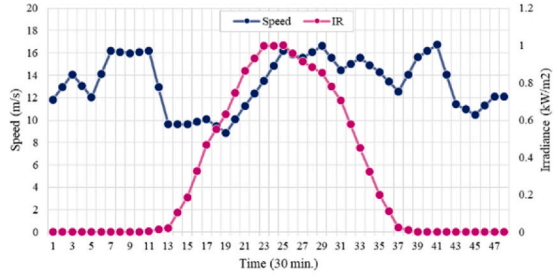

(h) Wind speed and solar radiation

Fig. 6. Input parameters for system operator and smart prosumers.

Table 5
Operational results for system operator in scenario 1.

Networks	Assets Operation ($)	Load Shedding ($)	Exchanges ($)				Sum ($)
			Upstream Grids	Smart Prosumers			
				Industrial Park	Charging Station	P2H Unit	
Power	–	71690.51	2042.19	0	0	0	73732.7
Gas	6151.27	0	1737.81	0	–	–	7889.08
Total	6151.27	71690.51	3780	0	0	0	81621.78

Table 6
Operational results for system operator in scenario 2.

Networks	Assets Operation ($)	Load Shedding ($)	Exchanges ($)				Sum ($)
			Upstream Grids	Smart Prosumers			
				Industrial Park	Charging Station	P2H Unit	
Power	–	47029.74	1477.42	0	0	0	48507.16
Gas	6151.27	0	1737.81	0	–	–	7889.08
Total	6151.27	47029.74	3215.23	0	0	0	56396.24

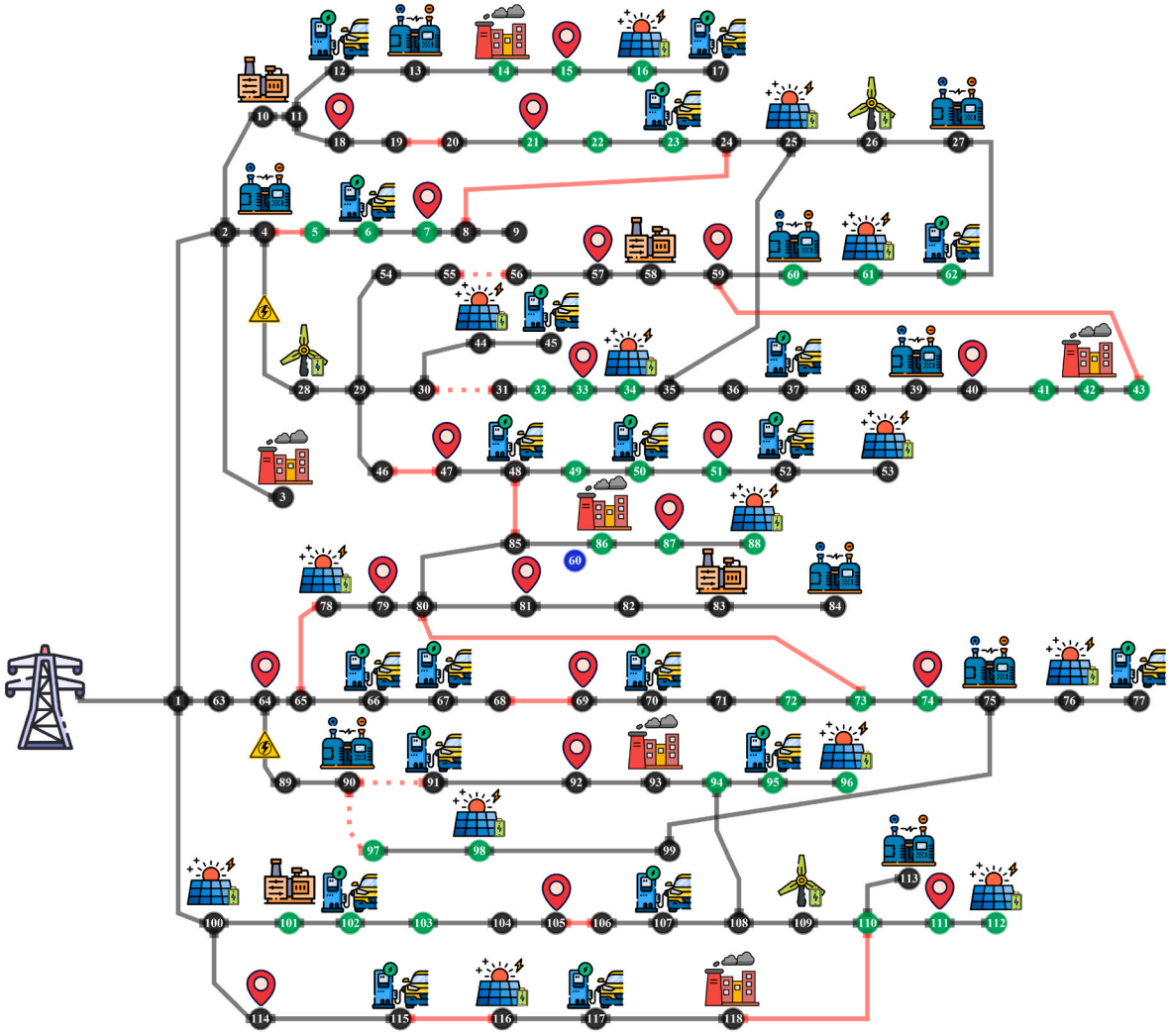

Fig. 7. Electricity network topology after dynamic switching.

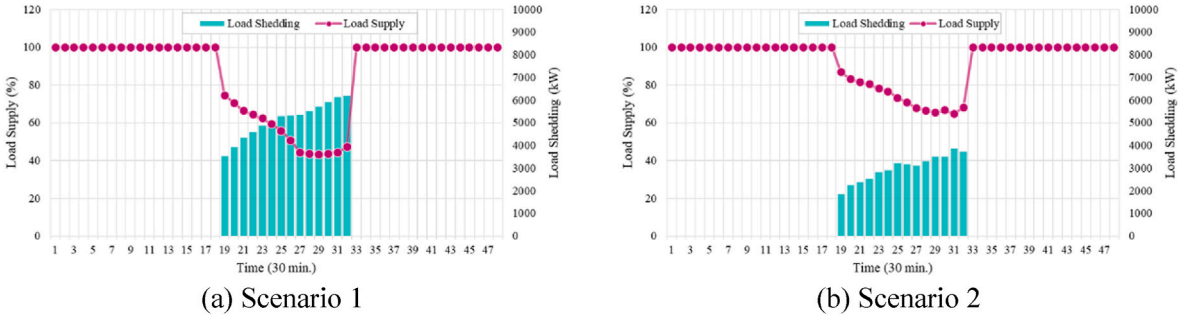

Fig. 8. Load supply rate and load shedding of critical loads.

Table 7
Operational results for system operator in scenario 3.

Networks	Assets Operation ($)	Load Shedding ($)	Exchanges ($)				Sum ($)
			Upstream Grids	Smart Prosumers			
				Industrial Park	Charging Station	P2H Unit	
Power	–	38318.28	1477.42	0	0	5729.48	45525.18
Gas	6151.27	0	1737.81	0	–	–	7889.08
Total	6151.27	38318.28	3215.23	0	0	5729.48	53414.26

Table 8
Operational results for system operator in scenario 4.

Networks	Assets Operation ($)	Load Shedding ($)	Exchanges ($)				Sum ($)
			Upstream Grids	Smart Prosumers			
				Industrial Park	Charging Station	P2H Unit	
Power	–	29151.76	1477.42	1456.58	0	5729.48	37815.24
Gas	6151.27	0	1737.81	156.21	–	–	8045.29
Total	6151.27	29151.76	3215.23	1612.79	0	5729.48	45860.53

Table 9
Operational results for system operator in scenario 5.

Networks	Assets Operation ($)	Load Shedding ($)	Exchanges ($)				Sum ($)
			Upstream Grids	Smart Prosumers			
				Industrial Park	Charging Station	P2H Unit	
Power	–	25746.95	1477.42	1456.58	1198.67	5729.48	35609.1
Gas	6151.27	0	1737.81	156.21	–	–	8045.29
Total	6151.27	25746.95	3215.23	1612.79	1198.67	5729.48	43654.39

30.9 % compared to scenario 1. To evaluate the network topology after automatic switching, Fig. 7 is presented. This figure reveals that after the fault occurred, the system operator disabled lines 55 (between buses 55 and 56), 30 (between buses 30 and 31), 90 (between buses 90 and 91) and 96 (between buses 90 and 97) using switching, while activating tie-lines 1 (between buses 27 and 62), 6 (between buses 25 and 35), 8 (between buses 75 and 99) and 11 (between buses 94 and 108). This topology change has altered the path of the power flow, enabling the electrification of buses 56–62, 31–43, 91–96 and 97–99. It should be mentioned that the load on these buses was disconnected during the entire emergency period in scenario 1, as it was not possible to power them due to the outage of lines 27 and 88.

Fig. 8a and b show the load shedding of high-priority consumers and the load supply level of the electric network in scenarios 1 and 2. The comparison of these figures demonstrates that the availability of the dynamic switching option in scenario 2 increases the supply level of electrical network loads by 54.87 %–73.4 % during the emergency period, compared to scenario 1. Additionally, these figures show that the load supply level of high-priority consumers increases significantly in scenario 2 compared to scenario 1, which is crucial from both security and economic perspectives. It should be mentioned that the load shedding penalty for these loads is double that of normal loads for the system operator.

5.2. Scenarios 3-5

In scenarios 3 to 5, the participation of smart prosumers in self-healing planning is considered. The numerical results obtained from the simulation of these scenarios are presented in Tables 7–9. The numerical results in Table 7 indicate that the activation of P2H units in scenario 3 has led to a 18.52 % reduction in load shedding of the electric network compared to scenario 2. This reduction in load shedding has subsequently reduced the overall costs of the system operator by 5.28 % in scenario 3 compared to scenario 2.

Fig. 9a and b show the program obtained for the P2H unit coupled with bus 4. Fig. 9a illustrates the hydrogen sold to the system operator. This hydrogen is injected into the tracks under the control of the system operator to be subsequently converted into electricity and injected into

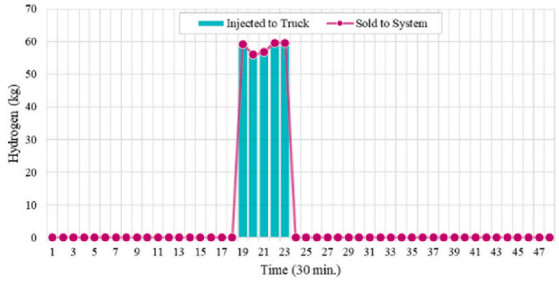

(a) Hydrogen sold to system operator

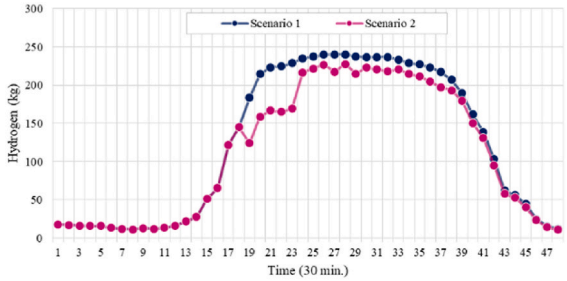

(b) Hydrogen sold to contracted customers

Fig. 9. Schedule obtained for a P2H unit.

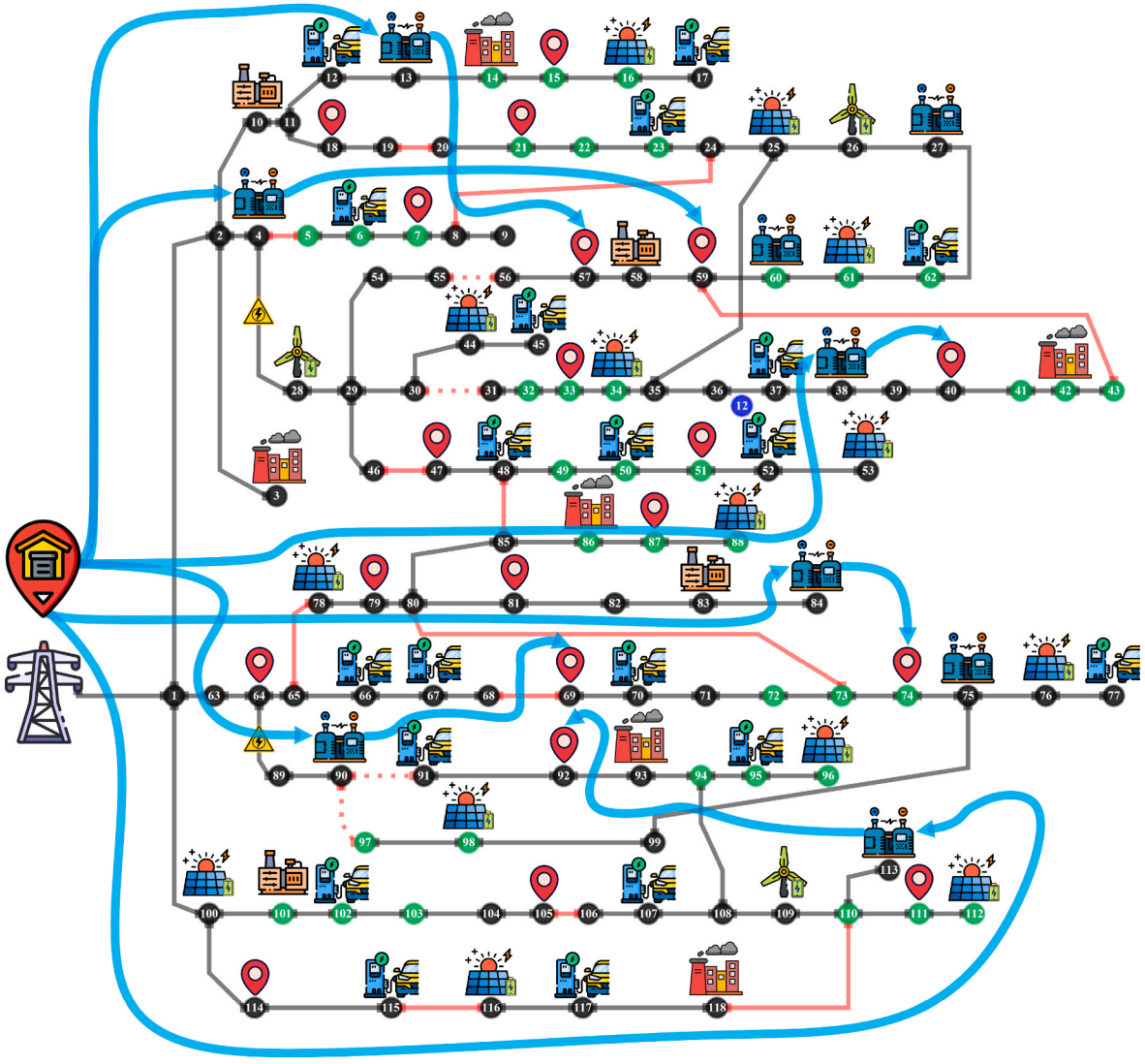

Fig. 10. Program obtained for fuel cell-equipped trucks in scenario 3.

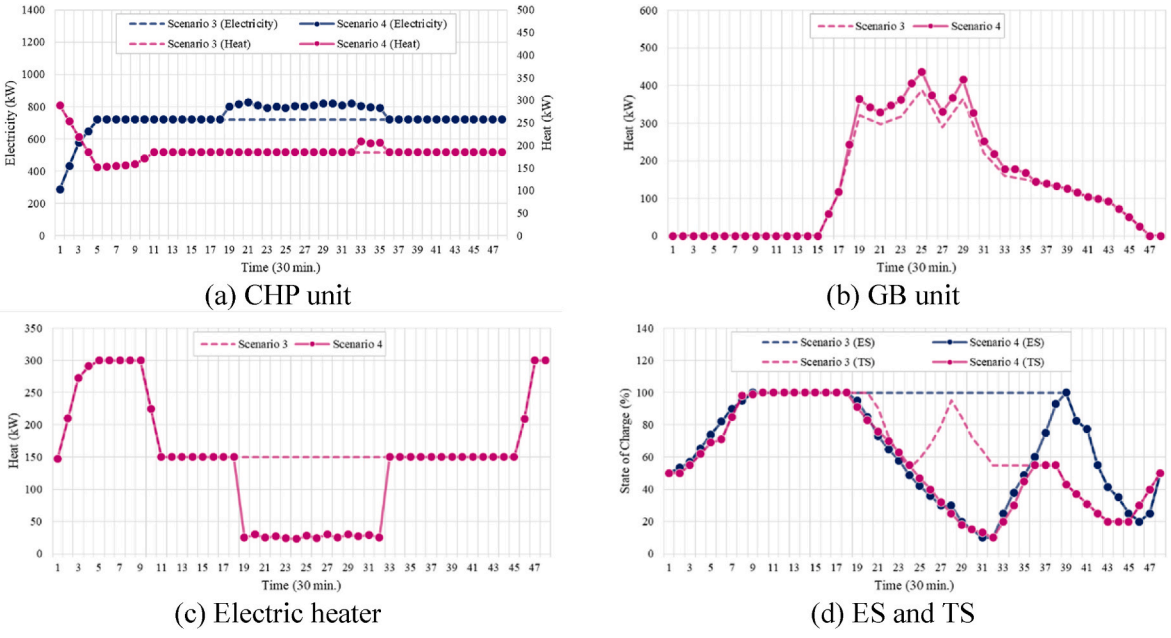

Fig. 11. Schedule obtained for the components of an industrial park.

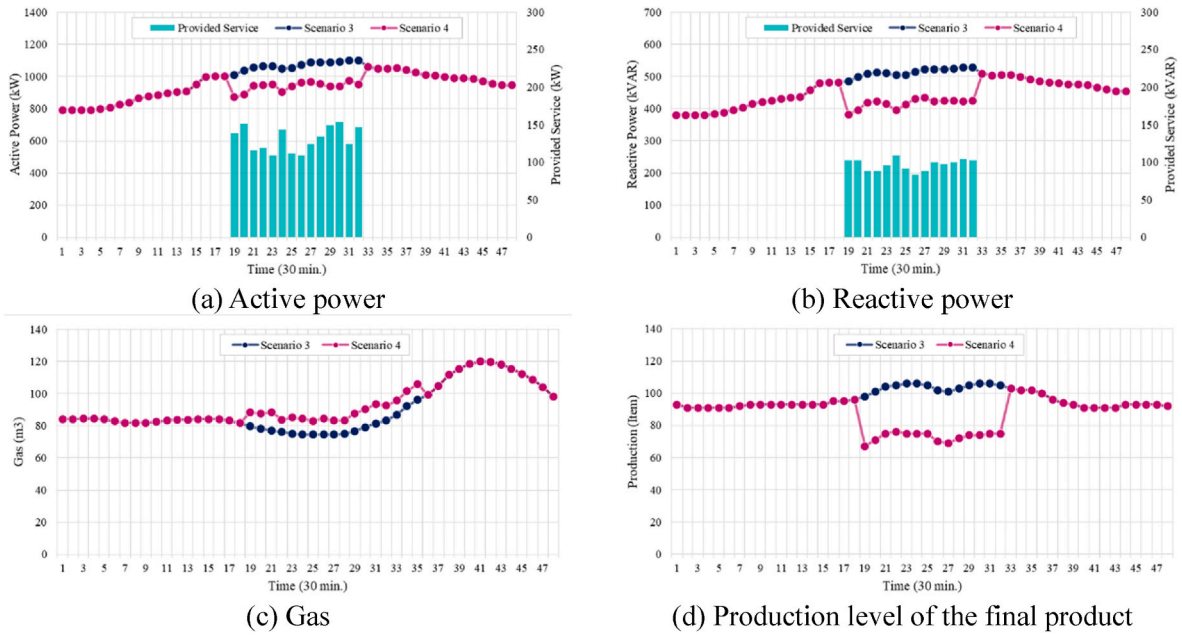

Fig. 12. Energy exchanges, emergency services and the production level of the final product in an industrial park.

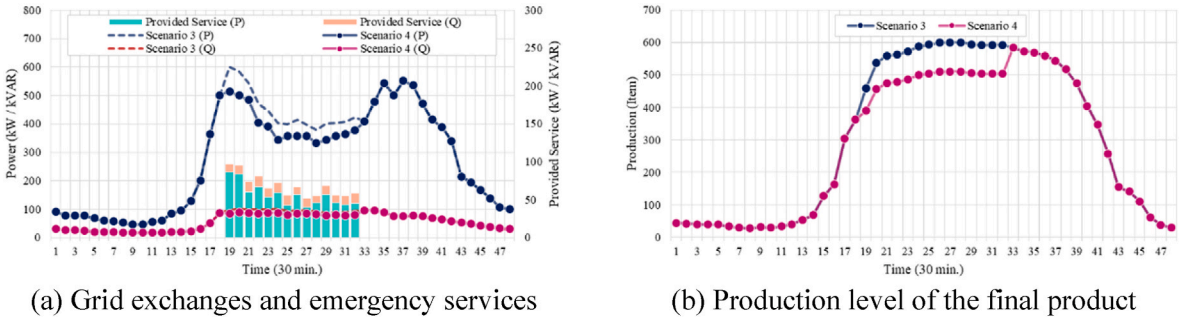

Fig. 13. Program of a charging station in scenarios 4 and 5.

the network. Fig. 9a also shows the hydrogen injected into the hydrogen tank of the trucks, with the amount being exactly equal to the hydrogen sold to the network at all times. Fig. 9b compares the hydrogen sold to customers under the P2H unit contract in scenarios 2 and 3. This figure reveals that the P2H sales schedule was similar during normal operating periods in both scenarios 2 and 3. However, the active participation of this P2H unit in self-healing planning in scenario 3 caused it to reduce part of its sales to contracted subscribers during the emergency period and instead sell to the system operator. It is worth noting that it is assumed each P2H unit can deviate by 35 % from its hourly sales plan. This deviation allowance enables P2H to cover the uncertainties caused by the production of its renewable wind and solar resources in normal operating conditions and provides services to the system operator in emergency operating conditions. Fig. 10 shows the program obtained for the trucks. As illustrated, the trucks went to the P2H units when the emergency started, and after loading the hydrogen, they went to the candidate points to convert it into electricity and inject it into the network.

In scenario 4, in addition to P2H units, industrial parks are also activated in self-healing planning. The numerical results of this scenario

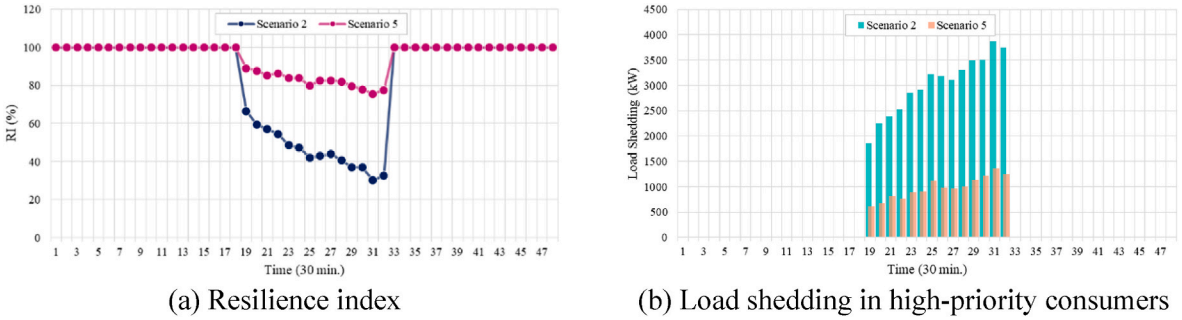

Fig. 14. Resilience index and load shedding in high-priority consumers.

Table 10
Operational results for system operator in scenario 6.

Networks	Assets Operation ($)	Load Shedding ($)	Exchanges ($)				Sum ($)
			Upstream Grids	Smart Prosumers			
				Industrial Park	Charging Station	P2H Unit	
Power	–	9886.33	3164.23	0	0	0	13050.56
Gas	1548.48	3583.12	0	0	–	–	5131.6
Total	1548.48	13469.45	3164.23	0	0	0	18182.16

Table 11
Operational results for system operator in scenario 7.

Networks	Assets Operation ($)	Load Shedding ($)	Exchanges ($)				Sum ($)
			Upstream Grids	Smart Prosumers			
				Industrial Park	Charging Station	P2H Unit	
Power	–	6678.57	3164.23	1192.68	0	0	11035.48
Gas	1548.48	1916.38	0	967.65	–	–	4432.51
Total	1548.48	8594.95	3164.23	2160.33	0	0	15467.99

are presented in Table 8 and show a 23.92 % reduction in load shedding and a 14.14 % reduction in total costs compared to scenario 3. The results indicate that although the system operator paid a total of $1612.79 for emergency services to industrial parks, the expenses related to load shedding were reduced by $9166.52 in scenario 4 compared to scenario 3.

Fig. 11a to d compare the operating points of the internal components of the industrial park connected to bus 93, including CHP, GB, electric heater, and ES and TS systems, in scenarios 3 and 4. Fig. 11a and b show that the operating points of the CHP and GB increased during the emergency period in scenario 4 compared to scenario 3. In contrast, Fig. 11c shows that the operating point of the electric heater decreased during the emergency period in scenario 4. The operator of the industrial unit tried to reduce the electric power received from the network by lowering the operating point of the electric heater. Fig. 11d shows that the ES and TS systems were discharged to their maximum limit during the emergency period to help supply the electrical and thermal loads of the industrial park.

Fig. 12a and b illustrates the industrial park's active and reactive power exchanges with electricity grid, as well as the active and reactive emergency power services it provided. It is worth mentioning that industrial parks provide active power services by changing the operating points of their generation units and production levels of their final products, while emergency reactive power services are provided by adjusting the settings of their CHP, renewable units, and capacitor banks. This figure shows that in scenario 4, when the industrial unit is activated in self-healing planning, it reduced its purchase of active and reactive power from the network during the emergency period and increased its gas purchase. This change is due to the increased operating points of CHP and GB units and the decreased operating point of the electric heater in the industrial park. Fig. 12c compares the industrial park's gas consumption in scenarios 3 and 4, illustrating its higher consumption in scenario 4, which is due to the increased operation points of CHP and GB units. Fig. 12d shows that the production level of the industrial park during the emergency period has decreased, allowing the operator to provide more capacity for emergency services.

In scenario 5, charging stations are also activated in self-healing planning along with P2H units and industrial parks, providing emergency services to the system operator. The numerical outputs of this scenario are presented in Table 9, showing that the activation of the charging stations has led to a 11.67 % reduction in load shedding and a 4.81 % reduction in the total operating costs of the system operator. During the emergency operation period, these stations enter emergency mode and charge cars to 85 % of their battery capacity instead of 100 %, thereby providing emergency services to the network.

Fig. 13a and b show the resulting program for the charging station connected to bus 37. Fig. 13a indicates that the purchase level of active and reactive power for this charging station decreased during the emergency period in scenario 5 compared to scenario 4. This figure shows that the difference between the power levels purchased in scenarios 4 and 5 was provided to the charging station operator as active and reactive power emergency services to the system operator. Fig. 13b also shows that the active participation of the charging station in self-healing planning in scenario 5 reduced its active power injected into cars during the emergency period compared to scenario 4. This reduction is due to the charging station entering emergency mode and charging cars up to 85 % of their battery capacity instead of fully charging them. It is worth mentioning that the charging station provides emergency reactive power services by changing the settings of its solar units and chargers.

Fig. 14a presents the system resilience index in scenarios 2 and 5. This figure shows that the active participation of all smart prosumers in self-healing planning in scenario 5 significantly increased the system resilience index compared to scenario 2 (without the participation of smart prosumers). Fig. 14b compares the load shedding level of high-priority consumers in scenarios 2 and 5. This figure reveals that the participation of smart prosumers in self-healing planning in scenario 5 significantly lowered the load shedding level of high-priority consumers compared to scenario 2.

5.3. Scenarios 6-8

In scenarios 6 and 7, self-healing planning is performed assuming that the electric network is operational and a technical problem occurs in the gas network. It is assumed that the volume of injected gas from station decreases by 25 % for a period of 5 h (from 02:00 p.m. to 6:00 p.m.). In scenario 6, self-healing planning is done without the participation of industrial parks, while in scenario 7, their participation is

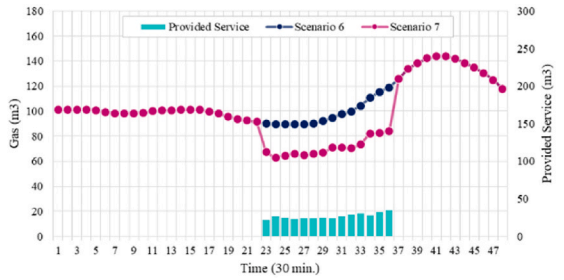

(a) Grid exchanges and emergency gas services provided by industrial park coupled with node 3

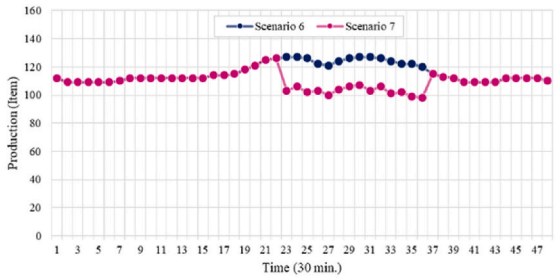

(b) Production level of the final product of industrial park coupled with node 3

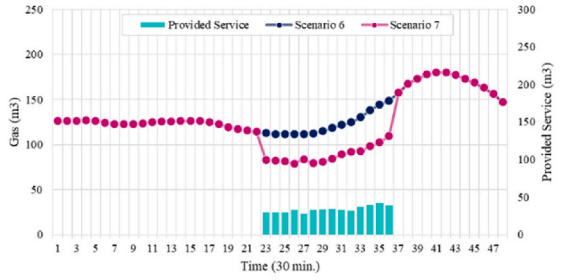

(c) Grid exchanges and emergency gas services provided by industrial park coupled with node 14

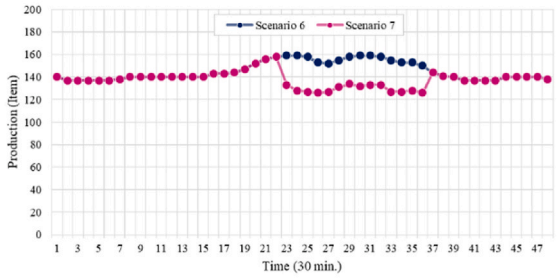

(d) Production level of the final product of industrial park coupled with node 14

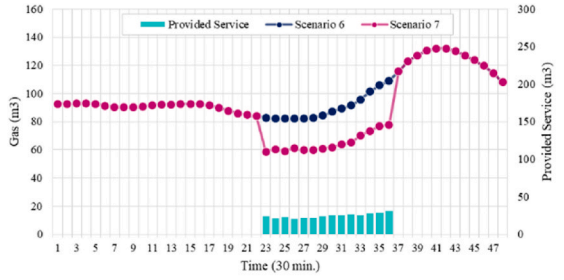

(e) Grid exchanges and emergency gas services provided by industrial park coupled with node 42

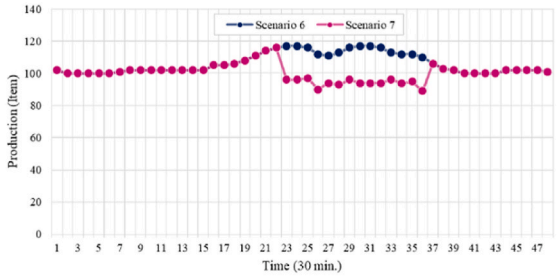

(f) Production level of the final product of industrial park coupled with node 42

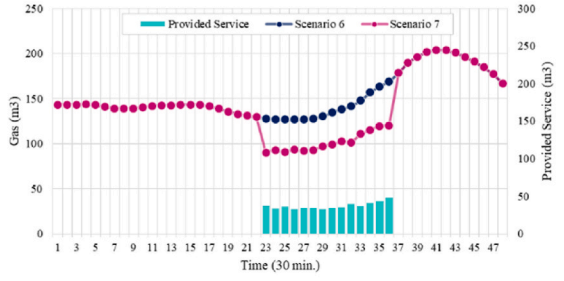

(g) Grid exchanges and emergency gas services provided by industrial park coupled with node 86

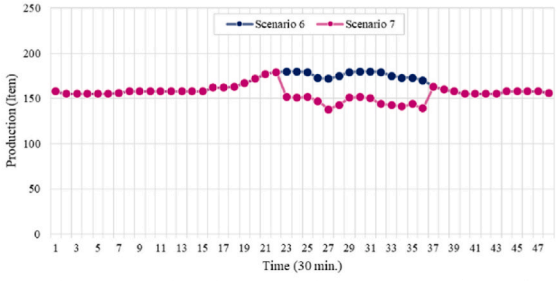

(h) Production level of the final product of industrial park coupled with node 86

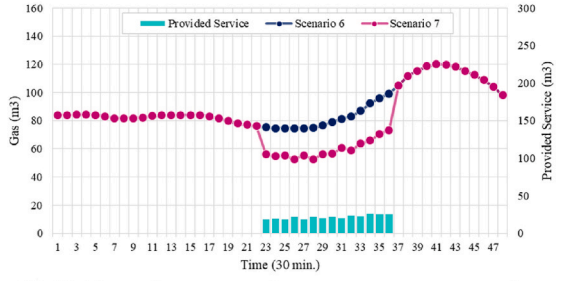

(i) Grid exchanges and emergency gas services provided by industrial park coupled with node 93

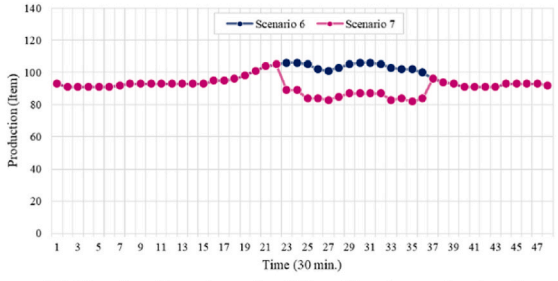

(j) Production level of the final product of industrial park coupled with node 93

Fig. 15. Programs obtained for smart prosumers in scenarios 6 and 7.

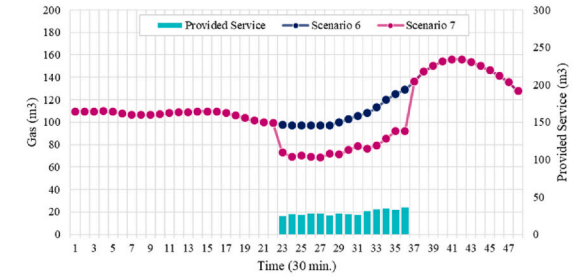

(k) Grid exchanges and emergency gas services provided by industrial park coupled with node 118

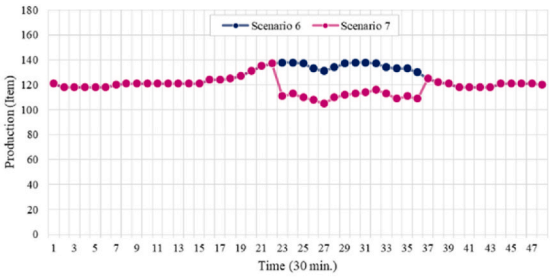

(l) Production level of the final product of industrial park coupled with node 118

Fig. 15. (*continued*).

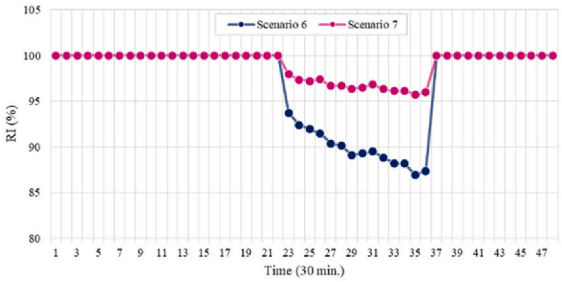

(a) Resilience index

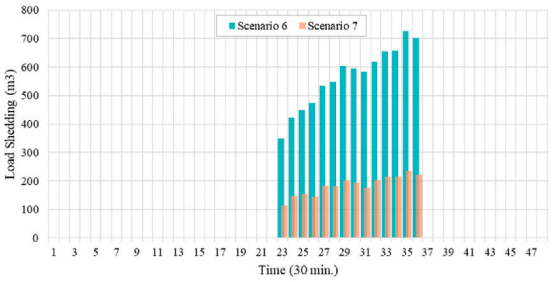

(b) Load shedding

Fig. 16. Load shedding and resilience index in scenarios 6 and 7.

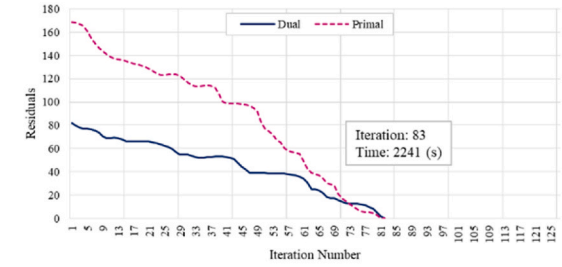

(a) Proposed augmented ADMM used in scenario 7

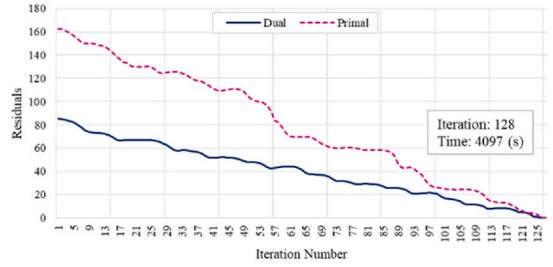

(b) Original ADMM used in scenario 8

Fig. 17. Results obtained for original and augmented versions of the ADMM algorithm.

considered. Since industrial parks are the only smart gas-consuming prosumers in this study, only their impact on scenarios 6 and 7 is investigated.

The results of scenarios 6 and 7 are presented in Tables 10 and 11, respectively. These results show that the participation of industrial parks in self-healing planning in scenario 7 reduces the load shedding of the gas network by 46.51 % and the total costs of the system operator by 14.92 %. According to Table 11, the system operator paid $967.65 for emergency gas services to the industrial parks and, in return, reduced the costs of load shedding in the gas network by $1666.74.

Fig. 15a–l show the emergency gas services provided by the industrial parks and the production levels of their final products. According to these figures, by reducing the production levels of their final products in scenario 7, industrial parks reduce the amount of gas purchased from the network during the emergency period and subsequently provide emergency gas services to the system operator. In Fig. 16a and b, the amount of load shedding in the gas network and the resilience index in scenarios 6 and 7 are compared. These figures show that the participation of industrial parks in self-healing planning in scenario 7 reduces the load shedding of the gas network throughout the emergency period and subsequently increases the resilience index level.

Scenario 8 is similar to scenario 7, with the difference that instead of the proposed augmented ADMM algorithm, the original ADMM algorithm is used for the coordination of prosumers and the system operator. Fig. 17a and b show the results obtained from the implementation of these algorithms. These figures show that although both versions achieve the global optimal solution, the proposed augmented ADMM algorithm converges with 83 iterations in 37.35 min, while the original version converges with 128 iterations in 68.28 min. These results demonstrate the much higher speed of the proposed augmented ADMM

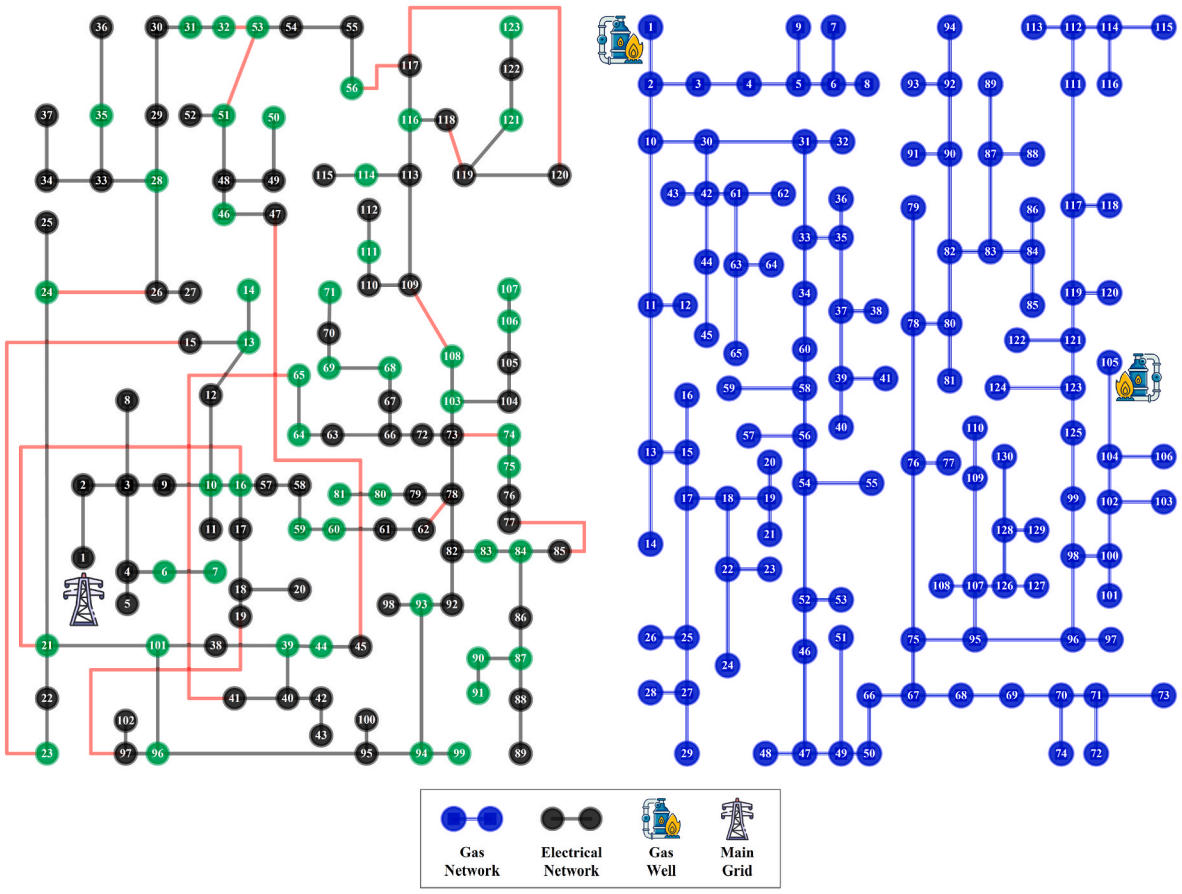

Fig. 18. Overview of the second test system [54,55].

compared to the original version, which is due to the dynamic update of the penalty coefficient of the ADMM algorithm by the logarithmic terms introduced in this proposed version.

5.4. Scenarios 9

Scenario 9 applies the proposed model to a large-scale system, as depicted in Fig. 18, comprising a modified 123-bus power distribution network [55] and a modified 130-node gas network (formed by coupling two 65-node gas networks) [54]. Table 12 provides the locations and capacities of smart prosumers and system components. Lines with automatic switches are shown in red, and critical loads in green. The simulated fault involves the outage of lines 24 (buses 16–57), 32 (buses 24–26), and 108 (buses 109–113) from 10:00 to 16:00.

Scenario 9 is solved under three modes: (1) deterministic fashion without grid-connected ES systems, (2) stochastic fashion without grid-connected ES systems, and (3) stochastic fashion with grid-connected ES systems. In the stochastic cases, all agents plan using scenario-based optimization to account for demand and renewable generation uncertainty, minimizing the expected cost across scenarios. Fig. 19a–h show the per-unit scenario profiles for loads and renewables, scaled by capacities in Table 12. For each uncertain parameter (wind speed, solar radiation, and load demand), 1000 scenarios were initially generated using Weibull, Beta, and Gaussian distributions, then reduced to five using the SCENRED tool in GAMS to ease computational burden.

Table 13 summarizes the numerical results for the three modes evaluated in Scenario 9. The introduction of uncertainties in Mode 2 led to a 10.12 % increase in system operator costs compared to the deterministic approach in Mode 1. Furthermore, enabling grid-connected ES systems in Mode 3 reduced load shedding by 6.34 % relative to Mode 2, resulting in a 4.55 % decrease in daily costs for the system operator. This improvement is attributed to the ability of the operator to utilize stored energy during emergencies.

Fig. 20a and b demonstrate that both the proposed augmented ADMM algorithm and its original version achieve global optimality under Mode 3 in Scenario 9. However, the augmented version converged in 94 iterations (2541 s), while the original required 152 iterations (4133 s), reflecting a 38.51 % reduction in solution time. When compared to the deterministic study, the scenario-based approach increased the number of iterations slightly, yet the overall solution time grew substantially. This is primarily due to the higher computational effort required for each agent's optimization in a scenario-based framework. Nonetheless, the solution time remains practical, particularly for the augmented algorithm.

Fig. 21 evaluates the contribution of each smart prosumer to system resilience, highlighting that industrial parks have the highest impact (56.62 %) due to their greater capacity and flexibility, followed by P2H units (24.97 %) and EV charging stations (18.4 %).

Additionally, four sensitivity analyses are presented in Fig. 22a–d, examining the effects of expanding smart prosumers and grid-connected

Table 12
Information on smart prosumers and network components.

Industrial Parks					
Unit Number		Connection Points			Production Capacity (item)
		Power	Gas		
1–5		8-12-27-29-54	3-8-114-89-119		130
6–10		38-72-105-110-120	79-61-34-80-56		160
11–15		20-77-82-98-102	15-23-130-108-68		110
P2H Units			Charging Stations		
Unit Numbers	Connection Points	Peak Demand (kg)	Unit Numbers	Connection Points	Peak Demand (kW)
1–5	15-30-37-49-70	300	1–10	25-33-36-47-48 52-55-115 118–122	600
6–9	73-76-79-113	250	11–17	4-9-58-66-104 109–112	800
10–13	18-22-88-95	200	18–27	26-42-45-66-78 85-89-92-97-100	700
Renewable Energy Resources					
Wind Units			Solar Units		
Unit Numbers	Connection Points	Capacity (kW)	Unit Numbers	Connection Points	Capacity (kW)
1–4	53-68-83-114	1200	1–11	6-10-23-39-60 74-81-84-87-101	500
5–8	3-21-44-99	1000	12–21	11-13-28-32-51 64-69-107-108 116–121	550
Storage Systems					
Energy Storage			Gas Storage		
Unit Numbers	Connection Points	Capacity (kWh)	Unit Numbers	Connection Points	Capacity (m^3)
1–4	53-68-83-114	300	1–11	6-10-23-39-60 74-81-84-87-101	600
5–8	3-21-44-99	400	12–21	11-13-28-32-51 64-69-107-108 116–121	800
Connection Points of Fuel Cell-Equipped Trucks					
7-14-16-24-31-35-46-50-56-59-65-66-71-75-80-82-85-89-90-93-94-96-103-106-113-123					

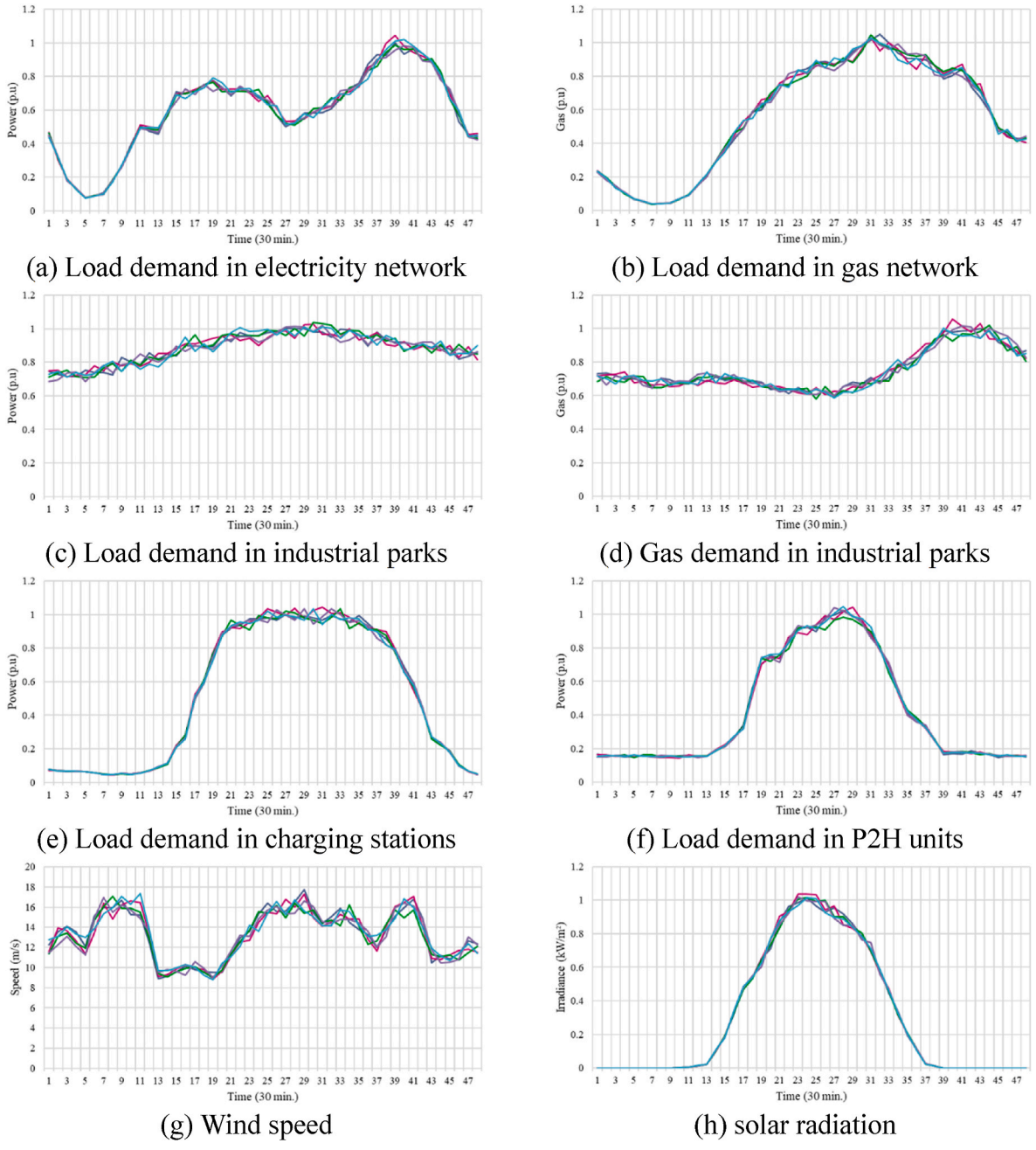

Fig. 19. Scenario profiles for loads and renewables in scenario 9.

Table 13
Operational results for system operator in scenario 9.

Mode 1: Deterministic Fashion - Without Grid-Connected ES Systems							
Networks	Assets Operation ($)	Load Shedding ($)	Exchanges ($)				Sum ($)
			Upstream Grids	Smart Prosumers			
				Industrial Park	Charging Station	P2H Unit	
Power	–	32441.42	1830.40	1914.95	1553.20	7383.93	45123.91
Gas	12440.01	0.00	3575.34	314.58	–	–	16329.93
Total	12440.01	32441.42	5405.74	2229.53	1553.20	7383.93	61453.84
Mode 2: Stochastic Fashion - Without Grid-Connected ES Systems							
Networks	Assets Operation ($)	Load Shedding ($)	Exchanges ($)				Sum ($)
			Upstream Grids	Smart Prosumers			
				Industrial Park	Charging Station	P2H Unit	
Power	–	37515.87	1943.69	2002.06	1641.03	7912.96	51015.61
Gas	13209.70	0.00	3884.48	335.47	–	–	17429.65
Total	13209.70	37515.87	5828.17	2337.53	1641.03	7912.96	68445.25
Mode 3: Stochastic Fashion - With Grid-Connected ES Systems							
Networks	Assets Operation ($)	Load Shedding ($)	Exchanges ($)				Sum ($)
			Upstream Grids	Smart Prosumers			
				Industrial Park	Charging Station	P2H Unit	
Power	–	35134.17	1800.67	2002.06	1641.03	7912.96	48490.89
Gas	12617.76	0.00	3884.48	335.47	–	–	16837.71
Total	12617.76	35134.17	5685.15	2337.53	1641.03	7912.96	65328.60

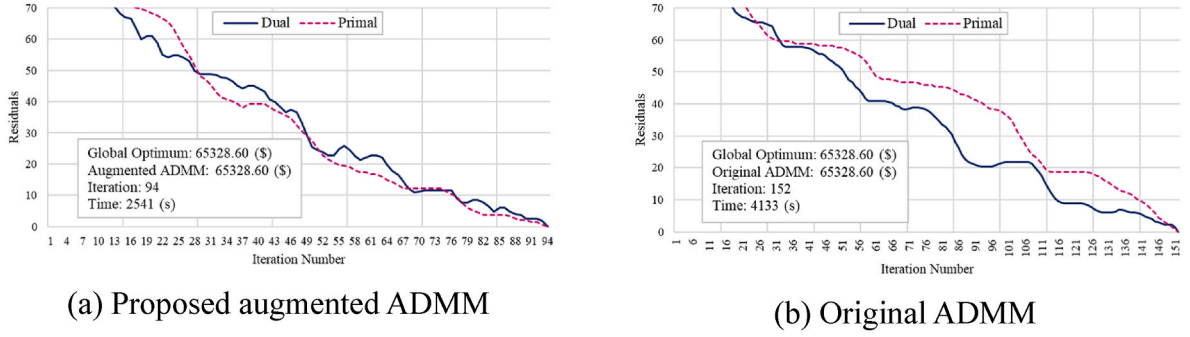

Fig. 20. Results obtained for original and augmented versions of the ADMM algorithm.

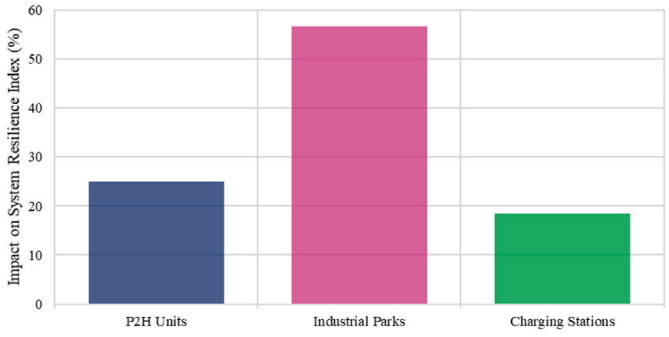

Fig. 21. Impact of smart prosumers on system resilience index.

ES systems on load shedding penalty, system operator costs, and the resilience index. The results indicate that increasing the deployment of smart prosumers and ES systems consistently reduces load shedding penalty and operational costs while enhancing system resilience.

Overall, the simulation results demonstrate that system operators and planners can significantly enhance grid resilience and minimize load shedding during emergencies by leveraging smart prosumer capacities and coordinated self-healing strategies. The findings suggest that integrating hydrogen storage, P2H units, and industrial parks not only optimizes resource allocation but also supports faster recovery, providing a robust framework for real-world applications in energy systems with high renewable penetration. These insights underline the practical value of the proposed mechanism in strengthening energy networks against disruptions and improving overall system reliability.

5.5. *Potential practical and computational limitations*

While the proposed two-stage optimization mechanism effectively enhances self-healing capabilities, certain practical and computational challenges may arise. The MIQCP format of the augmented ADMM optimization increases with the scale of the network and the number of smart prosumers, potentially impacting real-time responsiveness. Additionally, communication between the system operator and prosumers, though minimized, still relies on robust and secure channels to maintain efficiency and data privacy. Finally, real-world constraints, such as logistical challenges in deploying fuel cell-equipped trucks and synchronization issues, may require advanced computational solutions or distributed computing strategies for seamless implementation. Future research may focus on addressing these aspects to further enhance scalability and real-time adaptability.

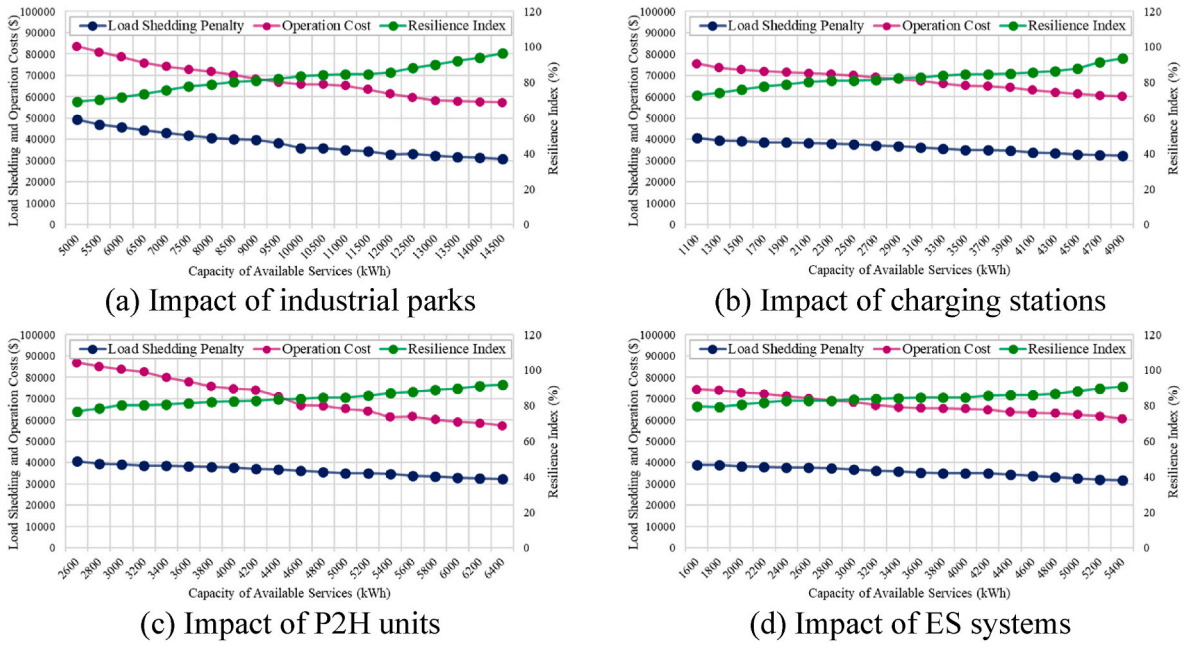

Fig. 22. Sensitivity analysis of smart prosumers and ES systems.

6. Conclusion

In this paper, a decentralized two-stage mechanism was presented to utilize the power, gas, and hydrogen capacities of smart prosumers, including industrial parks, P2H units, and charging stations, to increase the resilience of coordinated power and gas networks under emergency conditions. An augmented ADMM algorithm and a space-time network model were included in the proposed two-stage mechanism. The augmented ADMM algorithm ensured the distributed optimization of the operator and prosumers in a secure manner, while the space-time network model facilitated the dispatch of fuel cell-equipped trucks to sensitive points of the network, respecting transportation constraints and ensuring efficient exploitation. The proposed model was simulated under nine different scenarios using the GUROBI solver in GAMS, and its key results are summarized below:

- The presented two-stage structure enables the system operator to simultaneously utilize the capacities of smart prosumers, automatic switching, and fuel cell-equipped trucks to improve the resilience of coordinated electricity and gas networks under emergency conditions. As shown in the results, these options reduced load shedding and user costs by 64.08 % and 46.51 %, respectively, and improved the system's resilience index by 80.34 %.
- By using a time-space network model, the operator of coordinated electricity and gas networks was able to load fuel cell-equipped trucks at the location of P2H units and dispatch them to sensitive points of the system, taking into account both transportation and operational constraints. This mechanism reduced the load shedding by 18.52 %, subsequently improving the resilience index by 23.18 %.
- The proposed augmented ADMM algorithm enabled the system operator to determine the required capacities according to the emergency operating conditions and allowed smart prosumers to provide their flexible capacities based on capacity-price signals received from the system operator. The analysis of the results proved that the proposed augmented version not only achieved the global optimal solution but also had a much faster convergence speed than the original version of this algorithm, making it suitable for implementation in emergency operation conditions. This algorithm converged with 45 iterations less than the original version and subsequently reduced the solution time by 45.3 %.

In general, the simulation results confirmed that the proposed mechanism allowed the operator of the coordinated electricity and gas networks to fully utilize the potential of smart prosumers, fuel cell-equipped trucks, and automatic switching to enhance system resilience, while maintaining privacy and ensuring global optimality.

CRediT authorship contribution statement

Jie Chen: Writing – original draft, Software, Methodology, Conceptualization. **Weiyu Gu:** Writing – original draft, Validation, Supervision. **Yahya Z. Alharthi:** Validation, Software, Data curation. **Shoujun Huang:** Visualization, Resources, Investigation. **Seyed Amir Mansouri:** Software, Methodology, Conceptualization.

Declaration of competing interest

The authors declare that they have no known competing financial interests or personal relationships that could have appeared to influence the work reported in this paper.

Acknowledgements

The research is supported by the National Social Science Fund of China (22BJY062), Science and Technology Research Program of Chongqing Education Commission of China (KJQN202200607), Disaster Research Foundation of China (2019B07), and Anhui Provincial Natural Science Foundation (2208085MG191).

Data availability

Data will be made available on request.

References

[1] Farrokhifar M, Nie Y, Pozo D. Energy systems planning: a survey on models for integrated power and natural gas networks coordination. Appl Energy 2020;262:114567. https://doi.org/10.1016/j.apenergy.2020.114567.
[2] Fambri G, Diaz-Londono C, Mazza A, Badami M, Sihvonen T, Weiss R. Techno-economic analysis of power-to-gas plants in a gas and electricity distribution network system with high renewable energy penetration. Appl Energy 2022;312:118743. https://doi.org/10.1016/j.apenergy.2022.118743.

[3] Li Y, Zhang X, Gao W, Xu W, Wang Z. Operational performance and grid-support assessment of distributed flexibility practices among residential prosumers under high PV penetration. Energy (Calg) 2022;238:121824. https://doi.org/10.1016/j.energy.2021.121824.
[4] Zhang P, Mansouri SA, Rezaee Jordehi A, Tostado-Véliz M, Alharthi YZ, Safaraliev M. An ADMM-enabled robust optimization framework for self-healing scheduling of smart grids integrated with smart prosumers. Appl Energy 2024;363:123067. https://doi.org/10.1016/j.apenergy.2024.123067.
[5] Zhou Y. Climate change adaptation with energy resilience in energy districts—A state-of-the-art review. Energy Build 2023;279:112649. https://doi.org/10.1016/j.enbuild.2022.112649.
[6] Gržanić M, Capuder T, Zhang N, Huang W. Prosumers as active market participants: a systematic review of evolution of opportunities, models and challenges. Renew Sustain Energy Rev 2022;154:111859. https://doi.org/10.1016/j.rser.2021.111859.
[7] Li R, Yan X, Liu N. Hybrid energy sharing considering network cost for prosumers in integrated energy systems. Appl Energy 2022;323:119627. https://doi.org/10.1016/j.apenergy.2022.119627.
[8] Rodríguez-Vilches R, Martín-Martínez F, Sánchez-Miralles Á, Gutiérrez de la Cámara JR, Muñoz Delgado S. Methodology to assess prosumer participation in European electricity markets. Renew Sustain Energy Rev 2024;191:114179. https://doi.org/10.1016/j.rser.2023.114179.
[9] Gazijahani FS, Salehi J, Shafie-Khah M. A parallel fast-track service restoration strategy relying on sectionalized interdependent power-gas distribution systems. IEEE Trans Ind Inf 2023;19:2273–83. https://doi.org/10.1109/TII.2022.3180755.
[10] Vazinram F, Hedayati M, Effatnejad R, Hajihosseini P. Self-healing model for gas-electricity distribution network with consideration of various types of generation units and demand response capability. Energy Convers Manag 2020;206:112487. https://doi.org/10.1016/j.enconman.2020.112487.
[11] Nazar MS, Jafarpour P, Shafie-khah M, Catalão JPS. Optimal planning of self-healing multi-carriers energy systems considering integration of smart buildings and parking lots energy resources. Energy (Calg) 2023:128674. https://doi.org/10.1016/j.energy.2023.128674.
[12] Alasvand Javadi E, Joorabian M, Barati H. A bi-level optimization framework for resilience enhancement of electricity and natural gas networks with participation of energy hubs. Int J Electr Power Energy Syst 2022;142:108312. https://doi.org/10.1016/j.ijepes.2022.108312.
[13] Hou H, Tang J, Zhang Z, Wang Z, Wei R, Wang L, et al. Resilience enhancement of distribution network under typhoon disaster based on two-stage stochastic programming. Appl Energy 2023;338:120892. https://doi.org/10.1016/j.apenergy.2023.120892.
[14] Wang Y, Qiu D, Teng F, Strbac G. Towards microgrid resilience enhancement via Mobile power sources and repair crews: a multi-agent reinforcement learning approach. IEEE Trans Power Syst 2024;39:1329–45. https://doi.org/10.1109/TPWRS.2023.3240479.
[15] Mansouri SA, Nematbakhsh E, Ahmarinejad A, Jordehi AR, Javadi MS, Marzband M. A hierarchical scheduling framework for resilience enhancement of decentralized renewable-based microgrids considering proactive actions and mobile units. Renew Sustain Energy Rev 2022;168:112854. https://doi.org/10.1016/j.rser.2022.112854.
[16] Shi W, Liang H, Bittner M. Dynamic microgrid formation for resilient distribution systems considering large-scale deployment of mobile energy resources. Appl Energy 2024;362:122978. https://doi.org/10.1016/j.apenergy.2024.122978.
[17] Nourian S, Kazemi A. A two-stage optimization technique for automated distribution systems self-healing: leveraging internet data centers, power-to-hydrogen units, and energy storage systems. J Energy Storage 2024;85:111084. https://doi.org/10.1016/j.est.2024.111084.
[18] Rodriguez R, Osma G, Bouquain D, Ordoñez G, Paire D, Solano J, et al. Electrical resilience assessment of a building operating at low voltage. Energy Build 2024;313:114217. https://doi.org/10.1016/j.enbuild.2024.114217.
[19] Shibu NBS, Devidas AR, Balamurugan S, Ponnekanti S, Ramesh MV. Optimizing microgrid resilience: integrating IoT, blockchain, and smart contracts for power outage management. IEEE Access 2024;12:18782–803. https://doi.org/10.1109/ACCESS.2024.3360696.
[20] Mahmud K, Khan B, Ravishankar J, Ahmadi A, Siano P. An internet of energy framework with distributed energy resources, prosumers and small-scale virtual power plants: an overview. Renew Sustain Energy Rev 2020;127:109840. https://doi.org/10.1016/j.rser.2020.109840.
[21] Cano A, Arévalo P, Benavides D, Jurado F. Comparative analysis of HESS (battery/supercapacitor) for power smoothing of PV/HKT, simulation and experimental analysis. J Power Sources 2022;549:232137. https://doi.org/10.1016/j.jpowsour.2022.232137.
[22] Ma K, Yu Y, Yang B, Yang J. Demand-side energy management considering price oscillations for residential building heating and ventilation systems. IEEE Trans Ind Inf 2019;15:4742–52. https://doi.org/10.1109/TII.2019.2901306.
[23] Yang M, Jiang Y, Zhang W, Li Y, Su X. Short-term interval prediction strategy of photovoltaic power based on meteorological reconstruction with spatiotemporal correlation and multi-factor interval constraints. Renew Energy 2024;237:121834. https://doi.org/10.1016/j.renene.2024.121834.
[24] Yuqi J, An A, Lu Z, Ping H, Xiaomei L. Short-term load forecasting based on temporal importance analysis and feature extraction. Elec Power Syst Res 2025;244:111551. https://doi.org/10.1016/j.epsr.2025.111551.
[25] Rong Q, Hu P, Yu Y, Wang D, Cao Y, Xin H. Virtual external perturbance-based impedance measurement of grid-connected converter. IEEE Trans Ind Electron 2025;72:2644–54. https://doi.org/10.1109/TIE.2024.3436629.
[26] Rong Q, Hu P, Wang L, Li Y, Yu Y, Wang D, et al. Asymmetric sampling disturbance-based universal impedance measurement method for converters. IEEE Trans Power Electron 2024;39:15457–61. https://doi.org/10.1109/TPEL.2024.3451403.
[27] Ran L, Yu J, Ma Z, Liu C. Risk-based operation of plug-in electric vehicles in a microgrid using downside risk constraints method. Int J Veh Inf Commun Syst 2024;9:393–414. https://doi.org/10.1504/IJVICS.2024.142054.
[28] Niu X, Ma N, Bu Z, Hong W, Li H. Thermodynamic analysis of supercritical Brayton cycles using CO2-based binary mixtures for solar power tower system application. Energy (Calg) 2022;254:124286. https://doi.org/10.1016/j.energy.2022.124286.
[29] Li F-F, Xie J-Z, Fan Y-F, Qiu J. Potential of different forms of gravity energy storage. Sustain Energy Technol Assessments 2024;64:103728. https://doi.org/10.1016/j.seta.2024.103728.
[30] Shen F, Wu Q, Xu Y, Li F, Teng F, Strbac G. Hierarchical service restoration scheme for active distribution networks based on ADMM. Int J Electr Power Energy Syst 2020;118:105809. https://doi.org/10.1016/j.ijepes.2019.105809.
[31] Zhu R, Liu H, Yu W, Gu W, Sun L. Resilience-oriented operation of integrated electricity-natural gas systems using hydrogen enriched compressed natural gas. IEEE Syst J 2024:1–12. https://doi.org/10.1109/JSYST.2024.3354876.
[32] Wu H, Xie Y, Deconinck G, Yu C, Hou K, Sun J, et al. Distributed coordinated restoration of transmission and distribution systems with repair crews and Mobile emergency generators. IEEE Trans Power Syst 2024:1–13. https://doi.org/10.1109/TPWRS.2024.3394455.
[33] Wang K, Xue Y, Zhou Y, Li Z, Chang X, Sun H. Distributed coordinated reconfiguration with soft open points for resilience-oriented restoration in integrated electric and heating systems. Appl Energy 2024;365:123207. https://doi.org/10.1016/j.apenergy.2024.123207.
[34] Taheri B, Safdarian A, Moeini-Aghtaie M, Lehtonen M. Distribution system resilience enhancement via mobile emergency generators. IEEE Trans Power Deliv 2020;36:2308–19.
[35] Hughes W, Zhang W, Bagtzoglou AC, Wanik D, Pensado O, Yuan H, et al. Damage modeling framework for resilience hardening strategy for overhead power distribution systems. Reliab Eng Syst Saf 2021;207:107367. https://doi.org/10.1016/j.ress.2020.107367.
[36] Zhang G, Zhang F, Wang X, Zhang X. Fast resilience assessment of distribution systems with a non-simulation-based method. IEEE Trans Power Deliv 2021;1. https://doi.org/10.1109/tpwrd.2021.3077239.
[37] Zhang G, Zhang F, Zhang X, Wang Z, Meng K, Dong ZY. Mobile emergency generator planning in resilient distribution systems: a three-stage stochastic model with nonanticipativity constraints. IEEE Trans Smart Grid 2020;11:4847–59. https://doi.org/10.1109/tsg.2020.3003595.
[38] Ye Z, Chen C, Chen B, Wu K. Resilient service restoration for unbalanced distribution systems with distributed energy resources by leveraging Mobile generators. IEEE Trans Ind Inf 2021;17:1386–96. https://doi.org/10.1109/tii.2020.2976831.
[39] Liu X, Hou K, Jia H, Zhao J, Mili L, Mu Y, et al. A resilience assessment approach for power system from perspectives of system and component levels. Int J Electr Power Energy Syst 2020;118:105837. https://doi.org/10.1016/j.ijepes.2020.105837.
[40] Sedgh SA, Doostizadeh M, Aminifar F, Shahidehpour M. Resilient-enhancing critical load restoration using mobile power sources with incomplete information. Sustain Energy, Grids Networks 2021;26:100418. https://doi.org/10.1016/j.segan.2020.100418.
[41] Chen H, Li H, Lin C, Jin X, Zhang R, Li X. An integrated market solution to enable active distribution network to provide reactive power ancillary service using transmission–distribution coordination. IET Energy Syst Integr 2022;4:98–115. https://doi.org/10.1049/esi2.12051.
[42] Sun J, Zhang Z. A post-disaster resource allocation framework for improving resilience of interdependent infrastructure networks. Transport Res Transport Environ 2020;85:102455. https://doi.org/10.1016/j.trd.2020.102455.
[43] Ding T, Qu M, Wang Z, Chen B, Chen C, Shahidehpour M. Power system resilience enhancement in typhoons using a three-stage day-ahead unit commitment. IEEE Trans Smart Grid 2021;12:2153–64. https://doi.org/10.1109/tsg.2020.3048234.
[44] Li Z, Tang W, Lian X, Chen X, Zhang W, Qian T. A resilience-oriented two-stage recovery method for power distribution system considering transportation network. Int J Electr Power Energy Syst 2022;135:107497. https://doi.org/10.1016/j.ijepes.2021.107497.
[45] Mansouri SA, Rezaee Jordehi A, Marzband M, Tostado-Véliz M, Jurado F, Aguado JA. An IoT-enabled hierarchical decentralized framework for multi-energy microgrids market management in the presence of smart prosumers using a deep learning-based forecaster. Appl Energy 2023;333:120560. https://doi.org/10.1016/j.apenergy.2022.120560.
[46] Hosseini SE, Ahmarinejad A, Tabrizian M, Bidgoli MA. Resilience enhancement of integrated electricity-gas-heating networks through automatic switching in the presence of energy storage systems. J Energy Storage 2021:103662. https://doi.org/10.1016/j.est.2021.103662.
[47] Sheidaei F, Ahmarinejad A. Multi-stage stochastic framework for energy management of virtual power plants considering electric vehicles and demand response programs. Int J Electr Power Energy Syst 2020;120:106047. https://doi.org/10.1016/j.ijepes.2020.106047.
[48] Sun Y, Li Z, Shahidehpour M, Ai B. Battery-based energy storage transportation for enhancing power system economics and security. IEEE Trans Smart Grid 2015;6:2395–402. https://doi.org/10.1109/TSG.2015.2390211.
[49] Salehimaleh M, Akbarimajd A, Valipour K, Dejamkhooy A. Generalized modeling and optimal management of energy hub based electricity, heat and cooling

demands. Energy (Calg) 2018;159:669–85. https://doi.org/10.1016/j.energy.2018.06.122.
[50] Hui H, Bao M, Ding Y, Yan J, Song Y. Probabilistic integrated flexible regions of multi-energy industrial parks: conceptualization and characterization. Appl Energy 2023;349:121521. https://doi.org/10.1016/j.apenergy.2023.121521.
[51] Yu Q, Wang Z, Song Y, Shen X, Zhang H. Potential and flexibility analysis of electric taxi fleets V2G system based on trajectory data and agent-based modeling. Appl Energy 2024;355:122323. https://doi.org/10.1016/j.apenergy.2023.122323.
[52] Mansouri SA, Nematbakhsh E, Ramos A, Tostado-Véliz M, Aguado JA, Aghaei J. A robust ADMM-enabled optimization framework for decentralized coordination of microgrids. IEEE Trans Ind Inf 2024:1–10. https://doi.org/10.1109/TII.2024.3478274.
[53] Zhang D, Fu Z, Zhang L. An improved TS algorithm for loss-minimum reconfiguration in large-scale distribution systems. Elec Power Syst Res 2007;77:685–94. https://doi.org/10.1016/j.epsr.2006.06.005.
[54] Cavana M, Mazza A, Chicco G, Leone P. Electrical and gas networks coupling through hydrogen blending under increasing distributed photovoltaic generation. Appl Energy 2021;290:116764. https://doi.org/10.1016/j.apenergy.2021.116764.
[55] Chen K, Hu J, Zhang Y, Yu Z, He J. Fault location in power distribution systems via deep graph convolutional networks. IEEE J Sel Area Commun 2020;38:119–31. https://doi.org/10.1109/JSAC.2019.2951964.